Journal Pre-proof

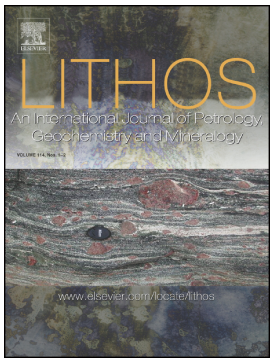

The Corno Alto complex (Adamello batholith): A modern analogue of the high Ba/K sanukitoids

A. Mosconi, E. Cannaò, F. Farina, M.G. Malusà, S. Zanchetta, M. Tiepolo

PII: S0024-4937(24)00034-3

DOI: https://doi.org/10.1016/j.lithos.2024.107522

Reference: LITHOS 107522

To appear in: *LITHOS*

Received date: 6 July 2023

Revised date: 25 January 2024

Accepted date: 25 January 2024

Please cite this article as: A. Mosconi, E. Cannaò, F. Farina, et al., The Corno Alto complex (Adamello batholith): A modern analogue of the high Ba/K sanukitoids, *LITHOS* (2023), https://doi.org/10.1016/j.lithos.2024.107522

This is a PDF file of an article that has undergone enhancements after acceptance, such as the addition of a cover page and metadata, and formatting for readability, but it is not yet the definitive version of record. This version will undergo additional copyediting, typesetting and review before it is published in its final form, but we are providing this version to give early visibility of the article. Please note that, during the production process, errors may be discovered which could affect the content, and all legal disclaimers that apply to the journal pertain.

© 2024 Published by Elsevier B.V.

Journal Pre-proof

The Corno Alto complex (Adamello batholith): a modern analogue of the high Ba/K sanukitoids

Mosconi A.[a,*], Cannaò E.[a], Farina F.[a], Malusà M.G.[b], Zanchetta S.[b], Tiepolo M.[a]

[a] Department of Earth Sciences "A. Desio", Università degli Studi di Milano, Via Botticelli 23, 21133 Milan, Italy

[b] Department of Earth and Environment Sciences, University of Milano-Bicocca, Piazza della Scienza 4, 1-20126 Milan, Italy

*Corresponding author: **angelica.mosconi@unimi.it**

E-mail addresses: enrico.cannao@unimi.it (Cannaò E.); federico.farina@unimi.it (Farina F.); marco.malusa@unimib.it (Malusà M.G.); stefano.zanchetta@unimib.it (Zanchetta S.); massimo.tiepolo@unimi.it (Tiepolo M.)

Journal Pre-proof

Journal Pre-proof

Abstract

The Corno Alto complex represents the onset of the intrusive igneous activity during the Alpine Orogen and for this reason has particular importance in the interpretation of the geodynamic evolution of the Alps. Whole-rock chemistry of the granitoid rocks of the Corno Alto complex reveals peculiar features with respect to the other units of the Adamello batholith, and to typical I-type and S-type granitoids. In particular, the Corno Alto rocks are enriched in Ba, Sr and La/Yb at any given SiO_2 content. U–Pb geochronology on zircon suggests an incremental assembly of the Corno Alto complex by multiple and possibly discrete magma injections in a time span of about 5 Myr starting from 44 Ma. The different zircon domains have significantly distinct Hf isotopic signature (up to 18 εHf units of variation) with some values trending towards the isotopic composition of the depleted mantle (DM). Bulk major and trace element geochemistry together with *in-situ* Hf isotope composition of zircon allow to distinguish at least two geochemically components in the Corno Alto rocks: i) a high Ba component characterised by high Sr and La/Yb ratios, likely derived from melting of carbonate sediments of slab origin; ii) a juvenile component with Hf isotopic signature close to the DM and capable to crystallize plagioclase with An_{90}, which is interpreted as the primitive mantle signal. This work constrains for the first time the occurrence of a slab derived carbonate input in the mantle-derived melts during the onset of the Alpine magmatism (dated at 44 Ma). The anomalously high thermal conditions required to induced carbonate melting may reflect the rise of asthenospheric material near the torn edge of the European slab where the Corno alto is located. Remarkably, these high thermal conditions parallel those at the Archean-Proterozoic transition and the Corno Alto complex could thus represent a kind of modern analogues of the high Ba/K sanukitoids.

Keywords: Corno Alto, Alpine orogen, Adamello batholith, High Ba-Sr granitoids

Journal Pre-proof

1. Introduction

Granitoids are the main component of the continental crust. The chemical composition of granitoids changed significantly during the early Earth's history (Laurent et al., 2014), with such a change reflecting variations in the mechanism of continental crust formation. A major shift occurred, in particular, at the Archean-Proterozoic boundary with the transition from the typical Archean sodic tonalite-trondhjemite-granodiorite association (TTG) to medium and high potassium post-Archean granitoids (Hawkesworth et al., 2020). In this period of transition, most cratons were also characterized by the occurrence of distinctive rocks called sanukitoids (Shirey and Hanson, 1984). These rocks, which define a complete magmatic series from diorites to granites, are enriched in LILE (*e.g.* Sr, Ba and LREE) and exhibit a moderately high concentration in compatible elements (*e.g.* Mg, Ni, and Cr). Sanukitoids are interpreted to mark the change in the site of partial melting from the subducting slab to the mantle wedge (Fowler and Rollinson, 2012) as a consequence of a modified tectono-thermal regime. The progressive cooling of the Earth definitely marked the decline of both TTG and sanukitoids leaving the scene to Phanerozoic granitoid rocks. However, occasionally, compositional equivalents of sanukitoids, known as "high Ba-Sr" granites, are recognized in late Cretaceous and late Cenozoic orogenic belts (Fowler et al., 2008). These modern analogues of Archean granitoids (both TTGs and felsic sanukitoids) likely formed in response to thermo-magmatic events producing thermal regimes similar to those dominating in the Archean and thus represent valuable proxies to shed light into the early evolution of the continental crust.

The Corno Alto complex, the oldest intrusion in the Tertiary Adamello batholith (Schaltegger et al., 2019) has been described as a TTG association (Lustrino et al., 2011). Being the oldest intrusion formed during the Alpine orogenesis, the Corno Alto complex is crucial to shed light into the tectono-magmatic conditions active at the onset of the Alpine magmatism, conditions that are not yet fully understood (*e.g.* Ji et al., 2019). Different models were proposed to account for magma generation during the Alpine Orogen such as post-collision lithospheric extension (Laubscher, 2010), slab-breakoff process (Blanckenburg and Davies, 1995) or progressive steepening of a continuous slab (e.g. Ji et al., 2019). In this frame, Ji et al. (2019) also suggested that, at the transition between the Alpine and Dinaric subductions, slab tear may have contributed to the genesis of adakite-like melts such as those reported in the Re di Castello Unit (Tiepolo and Tribuzio, 2005).

Despite the key importance of understanding the tectono-magmatic conditions at the onset of the Alpine Orogeny, the available geochemical and geochronological characterisation of the Corno Alto intrusive complex is not satisfactory.

This study aims to investigate the petrogenetic processes generating the early melts in the Alpine orogeny and their bearing on the general architecture of the Alpine evolution. We present a new comprehensive dataset combining whole-rock and *in-situ* zircon geochemistry and geochronology (U–Pb dates, trace element compositions and Hf isotopes) on different lithotypes of the Corno Alto complex. Geochemical data revealed a high Ba-Sr character of the complex, peculiar compared to the other Adamello units, which is discussed in the light of recent geodynamic constraints for the Alpine region.

2. Geological setting

The Adamello batholith is the largest and oldest intrusion in the Alpine belt emplaced along the Periadriatic fault system during the Eocene and the early Oligocene, after the subduction of the Neo-Tethys ocean and the subsequent collision between the paleo-European and paleo-African continental plates (e.g., Callegari and Brack, 2002; Fig. 1a-b). The Adamello batholith consists of discrete petrographically and isotopically distinctive plutons (Ulmer et al., 1983) of calc-alkaline affinity ranging in composition from quartz-diorite to granodiorite (Dupuy et al., 1982). Mafic rocks are locally associated with coeval felsic lithologies, both as satellite bodies at the pluton margins and as syn-plutonic intrusions (Blundy and Shimizu, 1991). Based on whole-rock radiogenic isotope data, the Adamello batholith is interpreted as evolved by assimilation and fractional crystallization from a picrobasaltic parental magma (Ulmer et al., 1983; Kagami et al., 1991). This model has been recently confirmed by *in-situ* Hf isotopes analyses in zircons from the different units of the batholith (Ji et al., 2019; Schaltegger et al., 2019).

The Corno Alto intrusive complex crops out in the eastern part of the batholith, close to the South Giudicarie Fault and includes the Sostino apophysis to the southeast (Fig. 1c-d). According to the literature, the complex is granodioritic to trondhjemitic in composition (Schaltegger et al., 2019) and intruded into a low-grade Variscan basement (Rendena Schists). Recent geochronological U–Pb data on zircons (e.g., Ji et al., 2019; Schaltegger et al., 2019) identified the Corno Alto intrusion as the oldest magmatic unit of the Adamello batholith with an average age of 43.47 ± 0.16 Ma. According to Relvini et al. (2022), the Corno Alto felsic rocks were formed by

mixing between anatectic melts, generated in the lower crust, and melts produced by fractional crystallization of mantle-derived magmas.

3. Sampling strategy and analytical methods

Location of the samples with GPS coordinates are reported in the Supplementary Table 1. Four main lithologies were identified and sampled in the Corno Alto complex, including the Sostino apophysis (Fig. 1c-d). A two-mica granodiorite (TMG) is the dominant lithology in the central and western part of the complex and nine samples were collected. Occasionally a porphyritic tonalite (PTN) and an equigranular tonalite (ETN), are found in the central and north-eastern part of the unit, respectively. Four representative tonalite samples were considered. An epidote-bearing granodiorite (EBG) dominates in the Sostino apophysis and four samples were considered in the study (Fig. 1d). Clear relationships between the different lithologies were not recognised in the field due to the extensive vegetation. For comparison purposes we also samples one diorite from a km scale body cropping out northwest to the Corno Alto pluton (MDR), and one tonalites (OTN) from the Mt. Ospedale area.

The selected samples were analysed for their whole rock major and trace element composition at the Central Analytical Facility (CAF) of the Stellenbosch University, South Africa. Major element compositions were determined on fused discs by X-ray fluorescence and bulk trace element concentrations were determined on the same materials by LA-ICP-MS. Major element compositions of rock-forming minerals (plagioclase, epidote) were measured at the Department of Earth Sciences “A. Desio” (ESD), University of Milano (Italy) by electron microprobe (EMPA). Zircon trace element composition and U–Pb dating were carried out by Laser-Ablation Inductively Coupled Plasma Mass Spectrometry (LA-ICP-MS) at the ESD. *In-situ* Hf isotope analyses were carried out on the same zircon domains selected for U–Pb dating, using LA MC-ICP-MS at ESD. Description of the analytical methods used are given in the Appendix A.

4. Petrography

4.*1 Two-mica granodiorites (TMG)*

Two-mica granodiorites are fine- to medium-grained and consist of plagioclase, quartz, biotite, K-feldspar and white mica (Table 1). Magnetite, titanite, apatite, and zircon are accessory phases. Plagioclase occurs as large individual crystals (up to 1 cm in size), commonly displaying embayed margins. Crystal cores with anorthite content up to An_{87} showing resorption margins are occasionally observed (Fig. 2a). These cores are overgrown by plagioclase with normal zoning down to An_{12} at the rim. Plagioclase also occurs in centimetric monomineralic glomerocrysts (Fig. 2b). These plagioclase crystals have cores with An_{30-50} and rims with An_{14-35} (Suppl. Table 2). Rarely, small crystals (< 400 µm) of epidote with pistacite content (Ps = $[Fe^{3+}/(Fe^{3+} + Al)]$ x100) of 27 mol% (Suppl. Table 2), and often showing allanite inner domains, were found hosted in plagioclase (Fig. 2c). Quartz, biotite, white mica and K-feldspars are mostly subhedral (Fig. 2d). Quartz also occurs in large grains (up to 4 mm) forming nodules that give a porphyric-like texture to the rocks.

4.2 Tonalites (ETN and PTN)

Tonalites are generally medium grained and consist of plagioclase, quartz, biotite, K-feldspar and magmatic epidote (Table 1). Accessory phases are magnetite, allanite, titanite, and zircon. Based on the rock texture, we distinguished equigranular tonalites (ETN) and pseudo-porphyric (PTN) tonalites. The latter are characterised by large plagioclase crystals or glomerocrysts (> 1 cm) dispersed in a fine-grained matrix (< 0.2 mm) consisting of plagioclase, quartz and biotite (Fig. 2e). Plagioclase composition in the PTN varies from An_{65} at the core to An_{25} towards the rim. Noticeably, few plagioclase crystals with cores up to An_{92} were also found.

In the ETN rocks, we observe the smallest range of An contents in plagioclase (An_{30-69}) with the highest values pertaining to the cores. Quartz and K-feldspar are interstitial between the other mineral phases. The dominant mafic phase is biotite, which has equilibrium contacts with the other rock-forming minerals (Fig. 2g). Epidote is a primary igneous phase and show sharp contacts with biotite, resorption textures with plagioclase and euhedral habit when hosted in biotite (Fig. 2g). Occasionally, epidote overgrowth euhedral allanite grains (Fig. 2h). All analysed grains have Ps between 26 and 30 mol%.

4.3 Epidote-bearing granodiorites (EBG)

Epidote-bearing granodiorites are the main rock type of the Sostino unit and are fine- to medium-grained. Major phases are plagioclase, quartz, biotite, K-feldspar and igneous epidote (Table 1). Apatite, titanite, zircon,

magnetite, and allanite are common accessory minerals. Texturally these rocks are almost equivalent to the two-mica granodiorites of the Corno Alto area. Glomerocrysts have plagioclase cores with An_{35-37} and rims with An_{13-22}. In comparison to the granodiorites from the Corno Alto area, the EBG have larger amounts of interstitial microcline, igneous epidote as mafic phase (Ps = 21.1 – 30.3 %) and no evidence of primary white mica (Fig. 2i).

4.4 Diorites (MDR) and Mt. Ospedale tonalites (OTN)

Diorites are medium to fine grained and consist of hornblende, plagioclase, biotite and quartz. Accessory minerals are zircon, apatite, and oxides (Table 1). Amphibole is fine-grained with acicular habit. Plagioclase (An_{42-56}) is subhedral and often shows resorbed boundaries and inclusions of hornblende and biotite grains. Biotite is subhedral to euhedral in habit and occurs both in association with hornblende and as inclusion in plagioclase crystals. Quartz is fine grained with anhedral habit.

The Mt. Ospedale tonalites have porphyritic texture and consists of amphibole, biotite and plagioclase dispersed in a finer grained matrix of quartz, biotite, plagioclase and microcline. Accessory minerals are apatite, zircon, titanite and oxides (Table 1). No systematic compositional differences are observed among the two plagioclase types, which vary from An_{41} to An_{73}.

5. Whole-rock geochemistry

Whole-rock major and trace element compositions of the Corno Alto rock suite are reported in Supplementary Table 1.

The Corno Alto and Sostino granitoids are calcic, with only a few samples that straddle the boundary with the calc-alkaline field (Fig. 3a). The granitoids are both metaluminous and peraluminous ($0.98 \leq A/CNK \leq 1.20$; Fig. 3b), silica-rich and ($65.3 \leq SiO_2 \leq 71.5$ wt.%, Fig. 3a) characterized by relatively low K_2O/Na_2O ratios (ranging from 0.35 to 0.80). According to the normative feldspar classification diagram for the granitoid rocks (An-Ab-Or, Barker, 1979), the Corno Alto and Sostino rocks plot on the granodiorite and tonalite fields (Fig. 3c) and follow a trondhjemitic trend in the ternary K-Na-Ca plot (Fig. 3d; e.g., Macera et al., 1983). Remarkably, although these rocks have been commonly referred to as “trondhjemites” in the literature (Macera et al., 1983;

Relvini et al., 2022), none of the studied samples plot in the trondhjemite field. Diorite and the Mt. Ospedale tonalite are metaluminous (A/CNK≤ 1.0) and less evolved (49.4 ≤ SiO_2 ≤ 62.9 wt.%) than the Corno Alto lithologies but with similar K_2O/Na_2O ratios.

Major element compositions (normalized to 100 wt.% anhydrous) were plotted in Harker diagrams using SiO_2 content on the *x*-axis (Fig. 4). The TMG rocks have the highest SiO_2 (≈70.0 wt.%) and display the lowest CaO (2.39- 3.25 wt.%), $Fe_2O_{3(tot)}$ (1.89-2.41 wt.%), MgO (0.62-0.84 wt.%), and TiO_2 (≈ 0.22 wt.%) contents. K_2O is quite variable, ranging from 1.58 to 3.14 wt.%. Mg# (Mg/(Mg+Fe)) is ≈ 0.40. TMG rocks represent the most peraluminous rocks with A/CNK ≥ 1.10 (Fig. 3b). Compared to the TMG, the EBG rocks have slightly lower SiO_2 contents (≈ 69 wt.%), similar Na_2O, K_2O and $Fe_2O_{3(tot)}$, but slightly higher CaO (up to 3.51 wt.%), TiO_2 (≈ 0.32 wt.%) and MgO (0.89-1.05 wt.%) contents. They are also characterized by a slightly metaluminous character (0.98 ≤A/CNK≤ 1.03; Fig. 3b). Both ETN and PTN rocks are less evolved in compositions, with SiO_2 ≈ 66 wt.%, and higher CaO (4.13-4.46 wt.%), Al_2O_3 (up to 17.9 wt.%), $Fe_2O_{3(tot)}$ (up to 3.93 wt.%), MgO (1.37-1.66 wt.%), and TiO_2 (≈ 0.40 wt.%) than the granodiorites. K_2O abundances are comparable to those of the less potassic TMG, while Na_2O and MnO are in the range of all the other rocks. Mg# is ≈ 0.45, similarly to the EBG rocks. The dioritic rocks (MDR) have lower SiO_2 (49.3 wt.%) and higher Fe_2O_3 (9.38 wt.%), CaO (9.11 wt.%), TiO_2 (1.32 wt.%) and MgO (9.72 wt.%) at comparable Al_2O_3, K_2O and Na_2O with the more evolved lithotypes of the CA unit. The Mt. Ospedale tonalite (OTN) is lower in SiO_2 (62.6 wt.%) and Na_2O contents (3.01 wt.%) compared to the CA tonalites.

The chondrite normalized REE patterns (Fig. A1 in the Appendix A) of the studied rocks are all characterized by strong enrichment in LREEs (up to 500 times chondrites) over HREEs (< 10 times chondrites). The $(La/Yb)_N$ ratio ranges from 14.2 to 30.7 in both TMG and EBG whereas is up to 61.2 in both types of tonalitic rocks (ETN and PTN). The Eu anomaly is almost negligible (Eu/Eu* ≈ 0.80-1.04). Diorites and the Mt. Ospedale tonalite (MDR and OTN) show less fractionated REE patterns ($[La/Yb]_N$: = 13.1-14.2) and a slightly more pronounced negative Eu anomaly (Eu/Eu* ≈ 0.76-0.93).

The primitive mantle normalized trace element pattern (Fig. 5a) is characterized by negative Nb, Ta, P, and Ti anomalies relative to the neighbouring elements and by enrichments in K, Pb, U, Th and LILEs (especially Sr and Ba; Fig. 5b). The highest Sr content (890 ppm) pertains to the PTN tonalitic rock whereas the equigranular tonalites (ETN), the epidote-bearing granodiorites (EBG) and the two-mica granodiorites (TMG) are

characterized by slightly lower contents (400-675 ppm) but still higher than those characterizing the diorites (MDR) and the Mt. Ospedale tonalites (OTN). The epidote-bearing granodiorites (EBG) are Ba-rich (1069-1614 ppm) and exhibit higher Pb, Th and U concentrations compared to the other rock types. The concentration of high-field strength elements (HFSE) is similar in the different rock types with the exception for the diorites (MDR) and Mt. Ospedale tonalites (OTN).

6. U–Pb zircon geochronology

At least two samples for each of the main lithologies of the Corno Alto complex were selected for U–Pb zircon geochronology, trace element and *in-situ* Hf isotope determinations. U–Pb ages and U–Pb Concordia diagrams are presented in the Supplementary Table 3 and Fig. A2 in the Appendix A. Analyses yielding >2% discordancy were not considered.

Based on CL properties, three different recurring domains, variably combined, were identified in zircons from the Corno Alto lithologies (Fig. 6). A-type domains are characterized by oscillatory zoning and medium- to low-luminescence. B-type domains are unzoned to weakly zoned, characterized by medium- to high-luminescence, often displaying a dissolution surface at their boundary. Finally, C-type domains have rounded boundaries and exhibit bright luminescence with no significant zoning. We anticipate that A- and B-type domains have ^{238}U-^{206}Pb ages that are identical within error . Therefore, in presenting ages, exclusive reference will be made to C-type domains. The U–Pb weighted mean ages of magmatic zircon grains are reported in figure 7.

6.1 Two-mica granodiorites (TMG)

Zircons from the two-mica granodiorites are prismatic to stubby, ranging in size from 75 μm to 400 μm. The length/width ratio is typically 2.5:1 to 4:1. Most of zircon grains have C-type and B-type cores mantled by domains with A-type texture. Only a subset of grains shows mostly A-type domains. In sample CA19-10, thirty-one analyses were carried out. Of these, nine analyses yield discordant dates and were discarded. Six analyses on inherited crystals (C-type textures) yielded dates ranging from 449 ± 9 Ma to 980 ± 20 Ma. The remaining twenty-four analyses on both cores and rims do not allow calculating a single mean concordia age. On a probability density plot the analyses reveal the occurrence of at least two distinct U–Pb age populations. Most of

the analyses define a main age peak at 39.1 ± 0.3 Ma (MSWD for c+e = 1; Fig. 7). A subset of A-type domains rimming C-type cores yield an older age peak at 43.4 ± 0.4 Ma (MSWD for c+e = 2.8). Fourteen analyses were performed on zircon grains of sample CA19-13. Of these, two analyses yield discordant ages. Twelve analyses yield concordant dates that allowed to calculate a mean concordia age at 43.6 ± 0.4 Ma (n=12, MSWD for c+e = 1.4). In sample CA19-37, twenty-five analyses were carried out. Of these, four analyses gave discordant dates whereas six analyses returned U–Pb ages ranging from 471 ± 12 Ma to 2461 ± 71 Ma. The remaining fifteen analyses suggest the occurrence of two zircon populations with distinct U–Pb ages: most of the analyses yield a mean concordant age of 41.7 ± 0.4 Ma (n=11; MSWD for c+e = 0.43), whereas few analyses gave an older mean concordant age at 44.4 ± 0.7 Ma (n= 4; MSWD for c+e = 0.25). Fifty-four analyses have been carried out on sample CA19-41. Eleven analyses returned discordant ages whereas fourteen analyses carried out on C-type domains gave old and highly variable ages, from 151 ± 7 Ma to 1068 ± 30 Ma. Most of the analyses yield a mean concordia age at 43.7 ± 0.3 Ma (n=21; MSWD for c+e = 1.3). A subset of eight analyses yielded younger mean concordia age at 41.4 ± 0.5 Ma (n=8; MSWD for c+e = 0.7).

6.2 Tonalites (ETN and PTN)

Zircons from tonalite rocks are mostly prismatic, rarely with stubby habitus. They range in dimensions from ~100 µm to more than 300 µm with a typical length/width ratio of 2.5:1. In sample CA19-16, (PTN) most of the zircon crystals display A-type domains in correspondence of both core and rim. Few zircon cores display B-type and C-type textures surrounded by A-type textures. Sixty-four analyses were carried out on the zircon grains from sample CA19-16. Of these, seven analyses were discordant. Five analyses on C-type domains returned dates spanning from 186 ± 4 Ma to 867 ± 19 Ma. Fifty analyses on both cores and rims revealed the occurrence of two populations with distinct U–Pb ages. Most of the analyses yield a mean concordant age at 41.9 ± 0.2 Ma (n= 37; MSWD for c+e = 0.79); another subset of fifteen analyses returned older concordant dates and a mean concordia age at 44.2 ± 0.3 Ma (n=14; MSWD for c+e = 0.75). Most of zircon crystals in sample CA19-21 (ETN) have A-type textures and only one core with C-type texture was found. Thirty-eight spot analyses in zircon grains from CA19-21 were performed. Of these, fifteen analyses are discordant. Twenty-three analyses yield a mean concordia age at 44.7 ± 0.3 Ma (n=23; MSWD for c+e = 0.7). One analysis performed on a C-type domain returned an age of 433 Ma ± 11 Ma.

6.3 Epidote-bearing granodiorites (EBG)

Most zircons from epidote-bearing granodiorites are prismatic, with elongated shape, sharp facets, and pointed tips. Zircon crystals are mainly colourless and transparent, with lengths ranging from 50 to 300 μm and length/width ratio of 2.5:1. In sample CA19-26, zircon grains have either A- and C-type cores. Forty-one analyses were carried out and of these, three analyses were discordant and ten analyses on C-type domains gave dates from 333 ± 18 Ma to 2174 ± 64 Ma. Twenty-eight analyses were concordant and yielded a mean concordia age at 44.0 ± 0.3 Ma (n=28; MSWD for c+e = 0.43). In sample CA19-30, all grains display cores and rims with A-type texture while no B- or C-type domains were found. Twenty-seven analyses were carried out and twenty-two analyses of both cores and rims yield concordant dates and returned a mean concordia age at = 44.3 ± 0.3 Ma (n=22, MSWD for c+e = 0.52).

6.4 Diorite (MDR)

Zircon grains from the diorite (CA19-3) are mostly fractured with fragments reaching 300 μm in size. Zircon CL textures are peculiar and cannot be classified into A- B- or C-type domains. Zircons are characterised by patchy textures with faint zoning and irregular longitudinal streak as well as occasional spongy textures at the core. Seventeen analyses were performed on zircon grains from sample CA19-3. Of these, one returned discordant date. Fifteen analyses yield a mean concordant age at 39.7 ± 0.4 Ma (MSWD for c+e = 0.56). One analyses on a zircon core gave a date at 44.8 ± 1.4 Ma.

6.5 Mt. Ospedale tonalite (OTN)

Zircons from the Mt. Ospedale tonalite (CA19-8) are prismatic to stubby, ranging in dimension from 70 to 300 μm, with length/width ratio of 2.5:1 to 4:1. Most of zircon grains are characterised by cores and rims with A-type texture. Twenty-two analyses were carried out and two analyses on C-type domains returned dates at 736 ± 36 Ma and 941 ± 54 Ma. The remaining twenty analyses on both cores and rims yielded a mean concordant age at 36.8 ± 0.4 Ma (n= 20; MSWD for c+e = 1.2). Remarkably, this age better agrees with the Adamello unit rather than to the older Corno Alto or Re di Castello unit (Ji et al., 2019).

Journal Pre-proof

7. Zircon geochemistry

7.1 Trace element compositions

Trace element composition was determined for several of the previously dated zircon domains and key compositional features are reported in figure 8. The full trace element characterisation is reported in Supplementary Table 3 and in Fig. A3). A-type domains show chondrite-normalized (McDonough and Sun, 1995) REE patterns, characterized by HREE enrichment [$(Lu/Gd)_N$ > 26-100], positive Ce anomaly, and negative Eu anomaly (Eu/Eu* down to ~ 0.4). These domains also have relatively high Nb, Ta (up to 86 ppm and 18 ppm, respectively) and U contents (~ 750-5550 ppm) while their Th/U ratio is low (< 0.5). B-type domains have REE patterns characterized by higher ΣLREE contents, a less pronounced HREE enrichment [$(Lu/Gd)_N$ ~ 9-40], positive Ce anomaly, and absent or slightly negative Eu anomaly (Eu/Eu* ~ 0.7). The concentrations in Nb and Ta are very low (up to a maximum of 10 ppm and 2.2 ppm, respectively), and Th/U values range between 0.80 to 1.72.

7.2 In-situ Hf isotopic compositions

In-situ Hf isotope composition of magmatic zircons was carried out on selected previously dated domains (Fig. 9; Supplementary Table 3). Zircon grains from the TMG show considerable variation in $\varepsilon Hf_{(i)}$ (-3.2 to +14.1) with a multimodal distribution of data characterized by the occurrence of at least three dominant clusters at around +3, +8, and +13. Interestingly, the higher $\varepsilon Hf_{(i)}$ values pertain to the B-type textural zircon domains. Zircon from the tonalitic rocks also have a large scatter in the $\varepsilon Hf_{(i)}$ isotopic composition, ranging between +2.5 and +13.0, with most of the values at ca. +6. The highest $\varepsilon Hf_{(i)}$ values are usually associated with B-type textural domains at the core of the grains (e.g., sample CA19-16, PTN). Noticeably, in sample CA19-21 (ETN), no $\varepsilon Hf_{(i)}$ values higher than +7 were measured. The zircons from the EBGs show a more restricted variation in the $\varepsilon Hf_{(i)}$ isotopic compositions with most of values giving a nearly unimodal distribution at ca. +5. Few data gave lower and higher values (down to -2.5 and up to +9.1). Most of the zircons from the MDR have $\varepsilon Hf_{(i)}$ values close to +6, with a few exceptions showing slightly negative value ($\varepsilon Hf_{(i)}$ down to -0.7). Noticeably, the old zircon core at 44 Ma shows $\varepsilon Hf_{(i)}$ at +12.0 ± 1.5 (2s). Negative $\varepsilon Hf_{(i)}$ values ranging from -3.2 to -9.6 are reported in the OTN sample.

Journal Pre-proof

8. Discussion

8.1 On the Corno Alto complex peculiarities in the framework of the Adamello batholith

The Corno Alto and Sostino granitoids have been described in the literature as an association of granodiorite and trondhjemite rocks (Macera et al., 1983; Relvini et al., 2022; Schaltegger et al., 2019), with distinct mineralogical and chemical features from the rest of the Adamello batholith. Here, we show that none of the granitoids in the Corno Alto and Sostino unit is a trondhjemite according to the Ab-An-Or normative diagram. Moreover, considering all the available data in the literature on the Corno Alto and Sostino rocks, only a very restricted number of samples effectively fall in the compositional trondhjemite field, with the vast majority being instead granodiorites and tonalites (Fig. 3c). The Corno Alto rocks have however some peculiar petrographic and geochemical features relative to the other units of the batholith, even if compared with rocks of similar age (e.g., south Re di Castello). Igneous epidote is relatively rare in metaluminous plutons (e.g. Narduzzi et al., 2017) but almost ubiquitous in the Corno Alto rocks. It occurs in place of amphibole, which is the main mafic rock-forming phase in the tonalites and granodiorites of the Adamello batholith (e.g., Callegari & Brack, 2002). Noticeably, in the oldest EBG rocks from Sostino, epidote occurs as inclusion into both plagioclase and biotite (Fig. 2c), thus suggesting early crystallization. According to experimental works, the stability of epidote in water-saturated metaluminous granitic systems is controlled by the pressure of crystallization and oxygen fugacity of the magma, with this phase forming at moderate to high pressures (0.6-0.8 GPa) in relatively oxidized magmas (Schmidt and Poli, 2004). Moreover, experimental studies have demonstrated that epidote dissolution in granitic magmas is relatively rapid (Brandon et a., 1996). Therefore, the survival of this mineral in calc-alkalic granitoids emplaced in the upper crust such as the Corno Alto implies rapid transport (e.g. Sial et al., 2008). This is also consistent with the occurrence of centimetric oscillatory-zoned plagioclase phenocrysts displaying albite-rich poikilitic rims with tiny quartz inclusions (Fig. 2f), interpreted as evidence of an initial slow crystallization followed by fast-cooling and intrusion into cooler regions of the lithosphere during the final stages of crystallization.

The Corno Alto granitoids also have a distinctive chemical composition. These rocks represent the most differentiated products of the Adamello batholith (Fig. 3a) showing the most peraluminous compositions (Fig. 3b) and, at any given SiO_2 content, the Corno Alto rocks have slightly higher Na_2O than most of the Adamello granitoids (Fig. 4). Exception is made only for a few SiO_2-rich rocks from the Val Fredda Complex (Re di

Castello unit) and W-Adamello (Blundy and Sparks, 1992; Dupuy et al., 1982; Macera et al., 1983; Ulmer et al., 1983). The trace element composition of the Corno Alto rocks reveals other peculiar features that include a strong Ba (Fig. 5) and, to a minor extent, Sr enrichment (Sr/Y > 40) as well as light-REE enrichment over HREE (La_N/Yb_N > 20) and Y, at any given SiO_2 content (see section 8.3).

8.2 Timing of assembly of the Corno Alto complex

The geochronological data presented in this work refine the current knowledge on the age of emplacement of the Corno Alto complex (Ji et al., 2019; Schaltegger et al., 2019) suggesting an assembly by multiple and possibly discrete magma injections in a time span of ~5 Myr (Fig. 7). U–Pb concordant data show the occurrence of three main recurring and distinctive age peaks at c. 44 Ma, c. 42 Ma, and c. 39 Ma (Fig. 10). The easternmost sector of the Corno Alto unit (Fig. 10a) exhibits the oldest ages with dates that are exclusively around ca. 44 Ma. These dates are equivalent to those reported by Schaltegger et al. (2019) and Ji et al. (2019) for the Corno Alto complex and likely represent the oldest igneous event in the Adamello batholith. The rocks dominating the central sector of the unit (Fig. 10c) show a relatively large age dispersion with a major peak at 42 Ma and a poorly defined inflection at 44 Ma. Noticeably, in the PTN sample the 42 Ma peak is statistically different from that at 44 Ma, which mostly results from the analysis of zircon cores (Fig. 10.c2). In this sample, no age distinction was observed between the different zircon types recognised under cathodoluminescence. The 42 Ma peak is thus interpreted as a second distinct and younger magmatic pulse, which likely assembled the central sector of the Corno Alto complex. Here, the 44 Ma domains are interpreted as antecrysts (e.g., Miller et al., 2007) – *i.e.* zircon grains crystallized from earlier magmatic pulses and mechanically incorporated into the intruding magma during emplacement. A youngest age cluster at 39 Ma, which is also distinct from the event at 42 Ma, characterises the lithologies of the western border of the complex (Fig. 10e). The occurrence of antecryst zircons at 44 Ma suggests that also this younger event recycled previous intrusions. The widespread occurrence of several inherited zircon grains of Proterozoic to Paleozoic age indicates extensive interaction of the magma with a host basement constituted by metasedimentary rocks in agreement with Boriani and Giobbi-Origoni (1982). The three magmatic pulses that assembled the Corno Alto complex are not distributed randomly but identify a trend of decreasing ages from the east to the west (Fig. 7). The progressive W-ward rejuvenation of the Corno Alto rocks could also potentially be interpreted as induced by partial resetting of the U–Pb zircon

system in response to the emplacement of the younger western Adamello units (e.g., Re di Castello North and Adamello). However, this alternative conflicts with the multiple zircon populations documented in our dataset (also within a single rock sample) characterizing the central sector of the unit. Because the W-ward trend of decreasing U–Pb ages is roughly perpendicular to the direction of the Giudicarie Fault (Fig. 1), which is located right above the European slab edge (Sun et al., 2019) possibly formed by tearing after interaction between the European and Dinaric slabs (Ji al., 2019; Malusà et al., 2021), we can thus identify a progressive migration of igneous activity in the Corno Alto complex away from the slab tear through time.

At the regional scale, it is noteworthy that the earliest magmatic events recorded in the Corno Alto rocks (at c. 44 Ma) also occur as xenocrystic zircon cores in the mafic rocks of the South Re di Castello unit (Tiepolo et al., 2011). This finding suggests that the onset of subduction-related igneous activity at 44 Ma in the Southern Alps was not restricted to the Corno Alto complex (D'Adda et al., 2011). It likely affected a wider crustal area, currently extending south-west towards the Val Fredda complex, paralleling the Giudicarie Fault and, thus, the trace of the European slab tear inferred on a geophysical ground (Malusà et al., 2021). In support of this conclusion is also the analogy in trace element composition and Hf isotopes of the B-type domains of the Corno Alto zircons with those of the Mt. Mattoni gabbro and Blumone hornblende-rich quartz diorite zircons (Broderick et al., 2015; Schoene et al., 2012), which strongly suggests a common origin. On the other hand, the A-type domains identified in the Corno Alto zircons also match the composition of the differentiated rocks of the Val Fredda complex, suggesting a common evolution with time of the entire crustal sector (Fig. 8). In this regard, the U–Pb ages of the Corno Alto and Val Fredda complexes fit the ages characterizing the youngest magmatic episodes of the intraplate Veneto Volcanic Province (VVP) in the Lessini Mts. and Val d'Adige, at ~51 Ma, ~45 Ma and ~42 Ma (Brombin et al., 2019; Visonà et al., 2007), which are also located along the inferred trace of the European slab tear.

8.3 Evidence for geochemically distinct sources at the origin of the Corno Alto complex

The granitoid rocks from the Corno Alto complex show the coexistence of at least two geochemically distinct components: i) a high Ba component characterized by high Sr and La/Yb ratios; ii) a juvenile component that crystallized high Ca plagioclase cores and zircon cores having $\varepsilon Hf_{(t)}$ signature approaching the depleted mantle (DM).

The high Ba-La/Yb component

The SiO_2 > 60 wt.% of the Corno Alto rocks, their Sr/Y > 40, and $(La/Yb)_N$ > 10 (Fig. 11a-b) recall the geochemical signatures of a particular group of arc related melts known as adakites (Defand and Drummond, 1990). In particular, the Corno Alto rocks have major and trace element compositional features (*i.e.*, Mg# ≈ 0.5, Na_2O > 3.5%, K_2O/Na_2O ratios ≈ 0.4, Y <18, Yb <1.8 ppm and Sr >400 ppm) that fulfil the criteria used by Martin et al. (2005) to define high-SiO_2 adakites (HSA). However, the extremely high Ba and, to a minor extent, Sr contents (≈1900 and 1100 ppm, respectively) shown by the Corno Alto suite are not entirely consistent with the composition of adakites, but resemble more closely the geochemical signature of a particular group of Phanerozoic rocks called 'high Ba-Sr granites' (Fowler and Rollinson, 2012). A key aspect in the interpretation of the high Ba (-Sr) signature of the Corno Alto rocks is relative to the mechanism responsible for the decoupling between Ba and K. In fact, at any given K_2O content, the Corno Alto granitoids have higher Ba concentrations than all the other rocks from the Adamello batholith (Fig. 11c). This feature cannot be the result of a process of close system fractional crystallization as Ba and K_2O are not separated from each other during the crystallization of plagioclase and/or biotite, which are the main minerals in the studied rocks (Table 1). Therefore, the enrichment in Ba (and Sr) calls for an external source. The whole-rock Sr-Nd isotope composition of the Corno Alto granitoids ($^{87}Sr/^{86}Sr_{(t)}$ up to 0.7064 and $\varepsilon Nd_{(t)}$ down to -3.81; Relvini et al., 2022) and the widespread occurrence of inherited zircon indicate that contamination with crustal-derived melts played an important role in the petrogenesis of the Corno Alto. However, we exclude that the peculiar high Ba-Sr signature observed is the result of a process of hybridization involving crustal melts derived by partial melting of the host basement. In fact, the low-grade Variscan metapelites (Rendena Schists) intruded by the Corno Alto do not possess high Ba contents (Bigazzi et al., 1986) and high La_N/Yb_N ratios. Moreover, melting of pelites at low pressure involves micas (biotite or muscovite), plagioclase and quartz as reactants (e.g. Grant, 2004) and lead to the formation of peritectic phases such as sillimanite and cordierite. None of these phases is capable of decoupling Ba from K. A multi-stage process of dehydration melting (and extraction of anatectic melts) of granulite-facies paragneiss was suggested by Sinigoi et al. (1994) to account for the high Ba and low K-Rb concentrations in the diorites of the Mafic Complex in the Ivrea Verbano Zone (Italy). Accordingly, melting of

granulite facies metapelites that have been depleted in K and Rb due to a previous event of partial melting in the lower crust might generate high-Ba melts.

Although it is impossible to completely discard this model, three lines of evidence argue against it. Firstly, the Corno Alto is the first intrusion of the Adamello batholith and a previous event of partial melting of the crust, at least during the Alpine orogeny, is undocumented. Secondly, recent phase equilibria models simulating a process of sequential melting of metapelites under fluid-absent conditions do not produce melt depleted in K even when temperatures of ca. 900°C are achieved (Mayne et al., 2020). Finally, restitic metapelites in the lower crust are commonly garnet bearing (Sinigoi et al., 1994), and their partial melting would impart to the melt a REE signature that contrasts with the spoon-shaped HREE pattern and the low Gd/Yb ratios of the Corno Alto rocks. Metapelite assimilation is thus unlikely the process at the origin of the Ba enrichment and its decoupling from K in the Corno Alto melts.

The K-Ba decoupling can be accomplished by involving minerals strongly discriminating elements by charge, i.e., capable of preferentially accept large 2+ cations (e.g., Ba^{2+} and Sr^{2+}) rather than 1+ cations (e.g., K^{+}) such as carbonates or sulphates. As apparent from the Ivrea Verbano crustal section (e.g., Bertolani, 1968), marbles and calcsilicate rocks are occasionally found in the mid/lower crust (Kinzigite Formation) of the Adria plate where the Adamello batholith intruded. However, in the Kinzigite Formation, carbonate-bearing rocks are significantly subordinated relative to the metapelites (e.g., Quick et al., 2002) and thus we do not retain that mid/lower crust carbonate-bearing rocks may have significantly contributed to the contamination process imposing the peculiar geochemical signature to the Corno Alto rocks. We propose a scenario where the Ba (and Sr) enrichment relative to K is a primary feature of the parental melt inherited from the mantle source. Partial melting of a metasomatized phlogopite-bearing mantle wedge would generate Ba and K-rich melts (Fowler et al., 2008), so it is discharged as possible process. Pelagic sediments were reported to be possibly extremely rich in Ba and Sr and also in LREE (e.g., Fowler et al., 2008; Plank and Langmuir, 1998). Barium and Sr in pelagic sediments are notably linked to biological productivity (i.e., barite precipitation) and biogenic phases (i.e., Sr in biogenic carbonates). Strontium is particularly abundant in Cenozoic carbonate oozes (up to 1500-2000 ppm) while it is relatively low in average shales (150-200 ppm). High Ba concentrations characterize proximal hydrothermal sediments where barite is commonly present, and sediments related to high biological productivity where barite is in association with organic matter and siliceous plankton (Plank, 2014). In figure 12a, the Ba-Sr

composition of the Corno Alto rocks is compared with that of several key drilled sections of present-day near deep-trenches worldwide, having different proportions of the diverse sedimentary constituents (Plank, 2014). The Corno Alto rocks are different from the pelitic- and terrigenous-dominated subducting trenches (e.g., Aleutians, Kamchatka, Sandwich) and define a trend pointing to the composition of a carbonate sediment cover of the slab (e.g., Columbia subducting trench). The Corno Alto rocks, in particular, parallel the Kermadec subducting sediment trench, which is characterized by high proportions of carbonate material closely resembling the composition of the Penninic units of the Tauern Window in the Eastern Alps (Fig. 12b-1 and 12b-2; Kurz et al., 1998). All the above pieces of evidence strongly suggest that the Ba enrichment shown by the Corno Alto rocks could be related to the involvement of a subducted carbonate-rich component in the source, as expected for the sediments deposited on top of the Neo-Tethyan oceanic crust.

The juvenile component

Evidence for the occurrence of a juvenile component into the petrogenesis of the Corno Alto rocks comes from trace element and *in-situ*-Hf isotopes. Zircon in the 44 Ma Sostino and ETN rocks are characterized by A-type textures and $\varepsilon Hf_{(t)}$ values close to +6 (±0.5 2SE). Zircon grains in all the other lithologies reveal multiple domains with both A-type and B-type (Fig. 6). $\varepsilon Hf_{(t)}$ values in A-Type domains are identical to those observed in the older rocks. B-type domains instead have highly positive $\varepsilon Hf_{(t)}$ values (up to +14), low incompatible elements concentrations (e.g., U, Nb, Ta) and a weak Eu anomaly, all features suggesting crystallisation from a juvenile melt whose $\varepsilon Hf_{(t)}$ is close to that of DM (Vervoort and Kemp, 2016). Noticeably, B-type domains are always at the core of the crystals and show resorption boundaries. Some B-type domains yield dates clearly older than the rim (e.g., MDR sample), in other cases the difference in age is below the analytical capability of the applied technique. In any case, the resorption boundary characterising B-type domains is evidence for their xenocrystic origin (Fig. 6). We thus suggest that at 44 Ma mantle-derived melts with a $\varepsilon Hf_{(t)}$ signature close to MORB, started crystallising at depth and were lately (42-39 Ma) mixed with younger igneous pulses. This is also in agreement with our finding of corroded An_{90} domains at the core of more albitic plagioclase crystals. Noticeably this process was already reported in the evolved rocks of the Re di Castello unit (Blundy and Shimizu, 1991). A-type domains, with high incompatible elements concentrations and deep negative Eu anomaly, likely crystallised from the same parental melt but after melt differentiation by fractional

crystallisation and assimilation of the shallow crust (e.g., Relvini et al., 2022), which is likely characterised by lower $\varepsilon Hf_{(t)}$.

8.4 Constraints on melt generation and geodynamic implications

The Corno Alto is the oldest intrusive complex of the entire Alpine Orogen (Ji et al., 2019) and represents the onset of the igneous activity related to the subduction of the Neo-Tethys ocean first and later the collision between the European and Adria continental plates. The Corno Alto complex has thus particular importance in the interpretation of the geodynamic evolution of the Alps. Many models were proposed to account for the long-lasting absence of magmatic activity during the Alpine Tethys subduction, whose beginning is approximately set at ~100‑95 Ma (e.g., Dewey et al., 1989; Malusà et al. 2015; Agard, 2021, and reference therein).

To constrain the petrogenesis of the high Ba-La/Yb component in the Corno Alto complex, a process capable of producing both the Ba enrichment and the La/Yb fractionation is required. Experimental studies indicate that Ba (and Sr) is highly soluble in the fluid phase (e.g., Kessel et al., 2005) compared to REE that are more prone to be retained in the solid residue of the slab. The presence of Cl in the system may enhance the mobility of several trace elements, including REE (e.g., Rustioni et al., 2021). However, being marine carbonates a Cl-poor system (e.g., Wang et al., 2020), the involvement of silicate hydrous melts or supercritical fluids is required for the REE transfer (Kessel et al., 2005; Fowler and Rollinson, 2012; Hermann and Rubatto, 2009). Alternatively, the influx of Cl-rich aqueous fluids deriving from the dehydration of slab serpentinites (*e.g.*, Barnes et al., 2018) may trigger the partial melting of the (meta)sedimentary cover situated atop the subducting slab, thus enhancing the Ba and LREE mobility. However, most of these models agree on the absence of sufficient fluids to promote partial melting in the mantle wedge (*e.g.*, Agard, 2021). This is consistent with the reconstructed cold path of Alpine subduction, very close to the so-called forbidden zone, as recorded by exhumed (U)HP rocks (Malusà et al. 2015). This evidence is reinforced by exhumed alpine high-P and ultrahigh-P metasedimentary rocks still retaining most of their volatile fraction (Busigny et al., 2003; Bebout et al., 2013; Garofalo, 2012). The onset of magmatism at 44 Ma, was likely triggered by the thermal perturbation induced by rising asthenospheric material along the slab tear located beneath the area encompassing the Adamello batholith, the Veneto Volcanic Province (VVP; NE Italy) and the Giudicarie Fault, and was subsequently sustained by a corner flow of asthenospheric

material during progressive slab steepening (Ji et al., 2019). Brombin et al. (2021) invoked a mechanism of asthenospheric poloidal flow to account for the middle Eocene magmatism in the VVP.

In this study, we showed that the parental melts of the Corno Alto complex likely record the presence of a component derived from the subducted carbonates, which is not occurring in all the younger units of the batholith. This evidence is essential in the interpretation of the evolution of the Alpine subduction because it implies a change with time in the sources activated for magma production. The loss of the carbonate input after 41 Ma may be explained by a change in the composition of the subducted material or, alternatively in the mechanism responsible for the element transfer from the slab to the mantle wedge.

The Alpine Tethys seafloor consisted of a complex assemblage of variably refertilized exhumed mantle rocks, irregularly distributed mafic magmatic rocks and pelagic sediments, together with ocean-continent transition lithosphere (OCT) domains and extensional allochthons (Malusà et al. 2018; Agard 2021). The slab compositional heterogeneities could therefore account for a sporadic carbonate input into the mantle wedge. However, the carbonate input does not recur in the younger units of the Adamello batholith as would be expected during the subduction of a compositionally heterogenous slab. It is worth noting that melt production is thought to start very close to the onset of continental collision in the Central Alps after complete consumption of the Tethyan ocean basin (e.g., Agard, 2021). Palinspastic reconstructions of the Alpine region consistently show that the inception of continental subduction migrated progressively from the Western to the Central Alps (Ford et al., 2006; Malusà et al., 2015), with the OCT lithosphere reaching the trench at ca 50-45 Ma (Malusà et al., 2018; Ji et al. 2019). Therefore, the formation of the Corno Alto marks the transition from oceanic subduction to the beginning of OCT subduction. In this scenario, the OCT subduction may lead to an increase in the terrigenous components in the subducting material, with this increase that should be clearly visible in the chemistry of the produced melts. A similar model was proposed by Tiepolo et al., (2014) that ascribed the difference in the chemistry between the amphibole-rich mafic rocks of the Adamello (Mt. Mattoni) and Bergell intrusions to differences in the composition of the subducting lithosphere. In particular, the enrichment in elements with high crustal affinity and the lower $\varepsilon Hf_{(t)}$ signature characterising the Bergell primary melts was related to the subduction of a thinned continental lithosphere. In the Adamello batholith the recognition of a terrigenous input in the source is difficult to assess mostly due to the superimposed effect of shallow level crustal contamination. Despite this limitation, we reckon that the similar Th/Nb ratio exhibited by these rocks of

the Corno Alto system and younger Adamello units of similar composition suggests that no significant changes in the terrigenous input have occurred (Plank, 2005).

The deep carbonate input characterizing the Corno Alto rocks is likely a consequence of a mechanism of element transfer from the slab to the mantle wedge, active only at the onset of the magmatism at 44 Ma. The thermal perturbation in response to the rise of asthenospheric material was particularly important near the torn edge of the European slab where the Corno Alto pluton is roughly located (Ji et al., 2019). Recent experiments revealed that under hydrous conditions temperatures in the range of 850 – 900 °C and 4.2 – 6 GPa (typical of warm subduction thermal conditions; Syracuse et al., 2010), may enhance partial melting of the carbonate fraction (Schettino and Poli, 2020). We thus propose that the high thermal conditions, in response to the asthenosphere upwelling, locally induced partial melting of the carbonate fraction of the sediment cover of the slab. Low-degree melting of carbonated sediments of slab origin were documented to be responsible of the strong enrichment in LREE of the mantle under the north China Craton (Chen et al., 2017). Carbonate melting thus can account also for the relatively high La/Yb ratios characterizing the Corno Alto melts. Interestingly, Zaccaria et al. (2021) found in the melt inclusions into zircon megacrysts of the middle Eocene VVP enrichments in BaO - SrO and evidence for S, and CO_2-rich fluids that were correlated to a source metasomatized by carbonatitic-kimberlitic liquids. The stringent analogy with the geochemical peculiarities found in the Corno Alto complex suggests a genetic link between the two complexes that is worth of detailed future investigations.

The high thermal conditions suitable for carbonate melting lasted approximately 5 Myr and were possibly at the origin of melts with adakitic signature reported in the Re di Castello unit (e.g., Tiepolo and Tribuzio, 2005). With the progressive lowering of the thermal conditions, slab dehydration become the dominant mechanism of element transfer from the slab to the mantle wedge. Being carbonate Hf-free, carbonate melting does not affect the $\varepsilon Hf_{(t)}$ signature of the mantle derived melts. We thus interpret the depleted $\varepsilon Hf_{(t)}$ signature found in the Corno Alto and approaching that of MORB (Vervoort et al., 2011), as reflecting the DM nature of the mantle source. Likely all the lower $\varepsilon Hf_{(t)}$ values found in zircon of the evolved Corno Alto lithologies reflect at various extent shallow level crustal contamination. Noticeably, depleted $\varepsilon Hf_{(t)}$ signatures also characterise zircons from the slightly younger products (39-41 Ma) of the southern Adamello (Ji et al., 2019; Schaltegger et al., 2019; Tiepolo et al., 2011), implying that no significant changes in the mantle source region have occurred. A larger

scale mantle source homogeneity is also testified by the occurrence of a DM signature in the igneous products of the VVP (Beccaluva et al., 2007; Bianchini et al., 2008) and interpreted as the mantle signature prior the subduction-related metasomatism (Brombin et al., 2019). This is further evidence for common inputs of deep asthenospheric mantle material in the source regions of the oldest Adamello products and the VVP (Fig. 13).

9. Implications for the genesis of the Archean and the post-Archean granitoids

The peculiar petrogenetic processes found at the origin of the Corno Alto complex suggest an alternative model for the petrogenesis of sanukitoids, which has implications for understanding the compositional transition between the Archean and the post-Archean granitoids. The petrogenesis of the Corno Alto complex has been traced back to a carbonate input in the source which transfers to the melt its distinctive high Ba/K ratio by hydrous-melts or supercritical fluids. The key factors for this process are thus a carbonate source of the metasomatic agent and the availability of thermal conditions high enough for the carbonate partial melting. During the Early Archean, although thermal conditions were sufficient for carbonate melting, carbonate inputs in subducting systems were almost negligible due to the paucity of carbonate marine organisms (Veizer & McKenzie, 2003; Ernst, 2009). Carbonate platforms began to appear during the late Archean but have become increasingly widespread since the Proterozoic and Phanerozoic when subduction thermal conditions do not reach the temperatures necessary for carbonate melting (Laurent et al., 2011). It follows that the full accomplishment of the conditions required for the genesis of the high Ba/K granitoids is mostly found at the Archean-Proterozoic transition. The anomalous thermal conditions (in the range of 850 – 900 °C and 4.2 – 6 GPa) pertaining to the Alpine subduction at 44 Ma apparently parallel those at the Archean-Proterozoic transition. The Corno Alto suite, as well as other Ba-Sr granites (Fowler and Rollinson, 2012), could thus represent a kind of modern analogues of the high Ba/K sanukitoids.

10. Conclusions

Major conclusions of the present study are the following:

- Granodiorites and tonalites, characterized by relatively low K_2O/Na_2O ratios, are the prevalent rock types of the Corno Alto complex and if compared with the rest of the Adamello batholith they show higher Na_2O, Ba, Sr and La/Yb ratios at any given SiO_2 and K_2O contents.
- U–Pb zircon geochronology reveals that the Corno Alto complex was assembled by multiple, and possibly discrete, magma injections at c. 44 Ma, c. 42 Ma, and c. 39 Ma. Noticeably, the oldest ages pertain to the easternmost side of the complex.
- Zircon and plagioclase reveal that at 44 Ma mantle-derived melts with a $\varepsilon Hf_{(t)}$ signature close to MORB crystallised at depth and were lately (42-39 Ma) recycled by younger magmatic pulses.
- Barium (and Sr) enrichments are a primary feature of the parental melt and related to the presence in the source of a deep carbonate input derived from the subducted slab. This geochemical signature is not occurring in all the younger units of the Adamello batholith and thus implies a change with time in the sources activated for magma production.
- We propose a scenario where the favourable thermal conditions for the partial melting of the subducted carbonates were established at onset of the Alpine magmatism (at 44 Ma) in response to the rise of asthenospheric material near the torn edge of the European slab, where the Corno Alto pluton is roughly located.

Journal Pre-proof

Acknowledgments

This work benefits funding from the Italian Ministry of University and Research (MUR) – Excellent Departments Projects. Gianluca Sessa is thanked for assistance during micro-analytical sessions. We thank A. Langone and an anonymous referee for criticism and comments, and Di-Cheng Zhu for careful editorial handling.

CAPTIONS TO FIGURES

Figure 1. a-b) Modified from Ji et al., (2019); c) Modified from Schaltegger et al. (2009); d) Modified from Carta geologica Provincia autonoma di Trento – Dati elaborati dal Servizio Geologico della provincia Autonoma di Trento (Sez. N. 59050-59010-59090).

Figure 2. a) Two plagioclase crystals of type 1 in TMG; b) Plagioclase glomerocryst in TMG; c) Epidote crystal enclosed in plagioclase in TMG; d) Lamellar primary white mica in TMG; e) big oscillatory zoned plagioclase in PTN; f) Tiny quartz crystals enclosed in the rim of plagioclase phenocrysts in PTN; g) Epidote euhedral inclusion in biotite in ETN; (h) Epidote overgrowth on allanite grains in ETN; i) Euhedral epidote grains in EBG.

Figure 3. a) A/CNK (A/CNK = Al / (2 Ca + Na + K) expressed as molar proportion atoms) vs. A/NK (A/NK = Al /(Na + K) expressed as molar proportion atoms) b) MALI index ($[Na_2O + K_2O]$ - CaO) vs. SiO_2 diagram; c) Normative An-Ab-Or diagram (after Barker, 1979) for Corno Alto plutonic rocks. d) Ternary K-Na-Ca plot. The classification curves are from Barker and Arth (1976). Literature data are SiO_2-rich Adamello rocks with SiO_2 > 56 wt.% (data from: Dupuy et al., 1982; Macera et al., 1983; Kagami et al., 1991; Blundy & Sparks, 1992; Ji et al., 2019; Relvini et al., 2022).

Figure 4. Major-element geochemistry of the Corno Alto and Sostino rocks compared with literature data (same as in figure 3).

Figure 5. Trace element composition of the Corno Alto rocks compared to the other Adamello rocks (the dashed patterns define the SiO_2-rich Adamello rocks with SiO_2 > 56 wt.%); symbols are the same of Fig. 3. a) Multi-element patterns normalized to Primitive Mantle (McDonough and Sun, 1995); b) Ba (ppm) vs. Sr (ppm) diagram for the Corno Alto rocks (coloured dots) and the other Adamello rocks (grey dots).

Figure 6. Cathodoluminescence images of representative zircon grains from the Corno Alto unit. U–Pb and εHf errors are reported as 2s.

Journal Pre-proof

Figure 7. Compilation of weighted average ages of zircon from the Corno Alto complex by laser-ablation ICP-MS. Error are reported as 2SE. The grey boxes represent the average of the 2σ error of each analysis.

Figure 8. Hf (ppm) *vs.* $(Lu/Gd)_N$ and Th/U *vs.* Eu/Eu^* diagrams from the Corno Alto zircons compared to Val Fredda (grey dots; Broderick et al. 2015) and the Veneto Volcanic Province (VVP) zircon crystals (green dots; from Visonà et al. 2007). Errors are within symbol.

Figure 9. Single zircon dates and Hf isotopes compositions from the Corno Alto and Mt. Ospedale rocks.

Figure 10. On left in image, geochronological results (U–Pb concordant data) for the Corno Alto rocks from the eastern (a), central (c) and western (e) parts of the Complex. On the right (b, d, f), distribution of $\varepsilon Hf_{(t)}$ values in zircon grains from the same rocks. Errors for Hf are reported as 2s.

Figure 11. Chondrite normalized (McDonough and Sun, 1995) $(La/Yb)_N$ vs. Yb_N (a) and Sr/Y vs. Y (ppm) (b) diagrams for the Corno Alto granitoids compared with classical island arc (light grey, Martin, 1999) and adakite fields (dark grey, Defant and Drummond, 1990); c) Ba (ppm) vs K_2O (wt.%) diagram showing the Ba-K decoupling for the Corno Alto rocks compared to literature data.

Figure 12.a) Ba/Sr ratio vs. Ba ppm for the Corno Alto rocks and bulk estimates for some complete sections near deep-trenches from all around the world (data from Plank, 2014). Grey field reports the variability of other Adamello rocks; b-1) Summary lithology subducting at each considered trench modified from Plank (2014); b-2) Representative stratigraphic section for the Tauern Window (modified after Kurz et al., 1998). Symbols are the same of Figure 11.

Figure 13. Modified from Ji et al., (2019). 3-D model showing the proposed relationships between slab steepening and Corno Alto magmatism (CA) in the absence of slab breakoff. The model highlight the influx of

the high Ba-La/Yb component deriving from subducted carbonate sediments. Projection of the Veneto Volcanic Province (VVP) is also shown (see text for details).

References

Agard, P., 2021. Subduction of oceanic lithosphere in the Alps: Selective and archetypal from (slow-spreading) oceans. Earth-Science Rev. 214, 103517. https://doi.org/10.1016/j.earscirev.2021.103517

Barker, F., Arth, J.G., 1976. Generation of trondhjemitic-tonalitic liquids and Archaean bimodal trondhjemite-basalt suites. Geology 4 (10), 596-600.

Barker, F., 1979. Trondhjemite: definition, environment and hypotheses of origin. In: Barker, F. (Ed.), Trondhjemites, dacites, and related rocks. DEV PETROL 6, pp. 1-12. https://doi.org/https://doi.org/10.1016/B978-0-444-41765-7.50006-X

Barnes, J.D., Manning, C.E., Scambelluri, M., Selverstone, J., 2018. The behavior of halogens during subduction-zone processes. role halogens Terr. Extraterr. geochemical Process. Surface, crust, mantle 545–590.

Bebout, G.E., Agard, P., Kobayashi, K., Moriguti, T., Nakamura, E., 2013. Devolatilization history and trace element mobility in deeply subducted sedimentary rocks: Evidence from Western Alps HP/UHP suites. Chem. Geol. 342, 1–20. https://doi.org/10.1016/j.chemgeo.2013.01.009

Beccaluva, L., Bianchini, G., Bonadiman, C., Coltorti, M., Milani, L., Salvini, L., Siena, F., Tassinari, R., 2007b. Intraplate lithospheric and sublithospheric components in the Adriatic domain: nephelinite to tholeiite magma generation in the Paleogene Veneto volcanic province, Southern Alps. In: Beccaluva, L., Bianchini, G., Wilson, M. (Eds.), Cenozoic Volcanism in the Mediterranean Area. Geological Society of America Special Paper, 418, pp. 131-152. https://doi.org/10.1130/2007.2418(07).

Bertolani, M., 1968. La petrografia della Valle Strona (Alpi occidentali italiane). Schweiz. Miner. petrogr. Mitt 48, 695–732.

Bianchini, G., Beccaluva, L., Siena, F., 2008. Post-collisional and intraplate Cenozoic volcanism in the rifted Apennines/Adriatic domain. Lithos 101, 125–140. https://doi.org/10.1016/j.lithos.2007.07.011

Journal Pre-proof

Bigazzi, G., Del Moro, A., Macera, P., 1986. A quantitative approach to trace element and Sr isotope evolution in the Adamello batholith (northern Italy). Contrib. to Mineral. Petrol. 94, 46–53.

Blanckenburg, F. Von, Davies, J.H., 1995. Slab breakoff: a model for syncollisional magmatism and tectonics in the Alps. Tectonics 14, 120-131.

Blundy, J.D., Sparks, R.S.J., 1992. Petrogenesis of mafic inclusions in granitoids of the adamello massif, Italy. J. Petrol. 33, 1039–1104. https://doi.org/10.1093/petrology/33.5.1039

Blundy, J.D., Shimizu, N., 1991. Trace element evidence for plagioclase recycling in calc-alkaline magmas. Earth Planet. Sci. Lett. 102, 178–197. https://doi.org/10.1016/0012-821X(91)90007-5

Boriani, A., Giobbi Origoni, E., 1982. Heat transfer in the thermo-metamorphic aureola of the northeastern sector of Mt. Adamello (Trento-Italy). Rend. SIMP 38, 3, 1251-1360.

Brandon, A.D., Creaser, R.A., Chacko, T., 1996. Constraints on rates of granitic magma transport from epidote dissolution kinetics. Science 271, 1845–1848

Broderick, C., Wotzlaw, J.-F., Frick, D., Gerdes, A., Ulianov, A., Günther, D., Schaltegger, U., 2015. Linking the thermal evolution and emplacement history of an upper-crustal pluton to its lower-crustal roots using zircon geochronology and geochemistry (southern Adamello batholith, N. Italy). Contrib. to Mineral. Petrol. 170. https://doi.org/10.1007/s00410-015-1184-x

Brombin, V., Bonadiman, C., Jourdan, F., Roghi, G., Coltorti, M., Webb, L.E., Callegaro, S., Bellieni, G., De Vecchi, G., Sedea, R., Marzoli, A., 2019. Intraplate magmatism at a convergent plate boundary: The case of the Cenozoic northern Adria magmatism. Earth-Science Rev. 192, 355–378. https://doi.org/10.1016/j.earscirev.2019.03.016

Brombin, V., Pettitt, E.A., Fahnestock, M.F., Casalini, M., Webb, L.E., Bryce, J.G., Bianchini, G., 2021. New geochemical and geochronological data on the Cenozoic Veneto Volcanic Province: Geodynamic inferences. Lithos 406–407, 106507. https://doi.org/10.1016/j.lithos.2021.106507

Busigny, V., Cartigny, P., Philippot, P., Ader, M., Javoy, M., 2003. Massive recycling of nitrogen and other fluid-mobile elements (K, Rb, Cs, H) in a cold slab environment: Evidence from HP to UHP oceanic metasediments of the Schistes Lustrés nappe (western Alps, Europe). Earth Planet. Sci. Lett. 215, 27–42. https://doi.org/10.1016/S0012-821X(03)00453-9

Journal Pre-proof

Callegari, E., Brack, P., 2002. Geological map of the Tertiary Adamello Batholitih (Northern Italy). Mem. di Sci. Geol. Padova 54, 19–49.

Chen, C., Liu, Y., Foley, S.F., Ducea, M.N., Geng, X., Zhang, W., Xu, R., Hu, Z., Zhou, L., Wang, Z., 2017. Carbonated sediment recycling and its contribution to lithospheric refertilization under the northern North China Craton. Chem. Geol. 466, 641–653. https://doi.org/10.1016/j.chemgeo.2017.07.016

D'Adda, P., Zanchi, A., Bergomi, M., Berra, F., Malusà, M.G., Tunesi, A., Zanchetta, S., 2011. Polyphase thrusting and dyke emplacement in the central Southern Alps (Northern Italy). Int. J. Earth Sci. 100, 1095–1113. https://doi.org/10.1007/s00531-010-0586-2

Defant, M.J., Drummond, M.S., 1990. Derivation of some modern arc magmas by melting of young subducted lithosphere. Nature 367, 662-665.

Dewey, J.F., Helman, M.L., Knott, S.D., Turco, E., Hutton, D.H.W., 1989. Kinematics of the western Mediterranean. Geol. Soc. London, Spec. Publ. 45, 265–283.

Dupuy, C., Dostal, J., Fratta, M., 1982. Geochemistry of the Adamello Massif (Northern Italy). Contrib. to Mineral. Petrol. 80, 41–48. https://doi.org/10.1007/BF00376733

Ernst, W.G., 2009. Archean plate tectonics, rise of Proterozoic supercontinentality and onset of regional, episodic stagnant-lid behavior. Gondwana Res. 15, 243–253.

Ford, M., Duchêne, S., Gasquet, D., Vanderhaeghe, O., 2006. Two-phase orogenic convergence in the external and internal SW Alps. J. Geol. Soc. London. 163, 815–826.

Fowler, M., Rollinson, H., 2012. Phanerozoic sanukitoids from Caledonian Scotland: Implications for Archean subduction. Geology 40, 1079–1082. https://doi.org/10.1130/G33371.1

Fowler, M.B., Kocks, H., Darbyshire, D.P.F., Greenwood, P.B., 2008. Petrogenesis of high Ba-Sr plutons from the Northern Highlands Terrane of the British Caledonian Province. Lithos 105, 129–148. https://doi.org/10.1016/j.lithos.2008.03.003

Garofalo, P.S., 2012. The composition of Alpine marine sediments (Bündnerschiefer Formation, W Alps) and the mobility of their chemical components during orogenic metamorphism. Lithos 128–131, 55–72. https://doi.org/10.1016/j.lithos.2011.10.009

Grant J.A., 2004. Liquid compositions from low-pressure experimental melting of pelitic rock from Morton Pass, Wyoming, USA. Journal of Metamorphic Geology, 22, 65-78.

Journal Pre-proof

Hawkesworth, C.J., Cawood, P.A., Dhuime, B., 2020. The evolution of the continental crust and the onset of plate tectonics. Front. earth Sci. 8, 326.

Hermann, J., Rubatto, D., 2009. Accessory phase control on the trace element signature of sediment melts in subduction zones. Chem. Geol. 265, 512–526. https://doi.org/10.1016/j.chemgeo.2009.05.018

Hogan, J.P., 1993. Monomineralic glomerocrysts: textural evidence for mineral resorption during crystallization of igneous rocks. J. Geol. 101, 531–540. https://doi.org/10.1086/648245

Ji, W.Q., Malusà, M.G., Tiepolo, M., Langone, A., Zhao, L., Wu, F.Y., 2019. Synchronous Periadriatic magmatism in the Western and Central Alps in the absence of slab breakoff. Terra Nov. https://doi.org/10.1111/ter.12377

Kagami, H., Ulmer, P., Hansmann, W., Dietrich, V., Steiger, R.H., 1991. Nd-Sr isotopic and geochemical characteristics of the southern Adamello (northern Italy) intrusives: Implications for crustal versus mantle origin. Journal of Geophysical Research: Solid Earth 96, B9, 14331-14346.

Kessel, R., Schmidt, M.W., Ulmer, P., Pettke, T., 2005. Trace element signature of subduction-zone fluids, melts and supercritical liquids at 120-180 km depth. Nature 437, 724–727. https://doi.org/10.1038/nature03971

Kurz, W., Neubauer, F., Genser, J., & Dachs, E., 1998. Alpine geodynamic evolution of passive and active continental margin sequences in the Tauern Window (eastern Alps, Austria, Italy): a review. Geologische rundschau, 87, 225-242.

Laubscher, H., 2010. Jura, Alps and the boundary of the Adria subplate. Tectonophysics 483, 223–239. https://doi.org/10.1016/j.tecto.2009.10.011

Laurent, O., Martin, H., Doucelance, R., Moyen, J.F., Paquette, J.L., 2011. Geochemistry and petrogenesis of high-K “sanukitoids” from the Bulai pluton, Central Limpopo Belt, South Africa: Implications for geodynamic changes at the Archaean-Proterozoic boundary. Lithos 123, 73–91. https://doi.org/10.1016/j.lithos.2010.12.009

Laurent, O., Martin, H., Moyen, J.F., Doucelance, R., 2014. The diversity and evolution of late-Archean granitoids: Evidence for the onset of “modern-style” plate tectonics between 3.0 and 2.5 Ga. Lithos 205, 208–235. https://doi.org/10.1016/j.lithos.2014.06.012

Journal Pre-proof

Lustrino, M., Duggen, S., Rosenberg, C.L., 2011. The Central-Western Mediterranean: Anomalous igneous activity in an anomalous collisional tectonic setting. Earth-Science Rev. 104, 1–40. https://doi.org/10.1016/j.earscirev.2010.08.002

Macera, P., G., F., A., P., E., C., 1983. A geochemical study on the acid and basic rocks of the Adamello batholith. Mem. Soc. Geol. It. 26, 223–259.

Malusà, M.G., Faccenna, C., Baldwin, S.L., Fitzgerald, P.G., Rossetti, F., Balestrieri, M.L., Danišík, M., Ellero, A., Ottria, G., Piromallo, C., 2015. Contrasting styles of (U) HP rock exhumation along the Cenozoic Adria-Europe plate boundary (Western Alps, Calabria, Corsica). Geochemistry, Geophys. Geosystems 16, 1786–1824.

Malusà, M.G., Frezzotti, M.L., Ferrando, S., Brandmayr, E., Romanelli, F., Panza, G.F., 2018. Active carbon sequestration in the Alpine mantle wedge and implications for long-term climate trends. Sci. Rep. 8, 4740.

Malusà, M.G., Guillot, S., Zhao, L., Paul, A., Solarino, S., Dumont, T., Schwartz, S., Aubert, C., Baccheschi, P., Eva, E., 2021. The deep structure of the Alps based on the CIFALPS seismic experiment: A synthesis. Geochemistry, Geophys. Geosystems 22, e2020GC009466.

Martin, H., Smithies, R.H., Rapp, R., Moyen, J.F., Champion, D., 2005. An overview of adakite, tonalite-trondhjemiten-granodiorite (TTG), and sanukitoid: Relationships and some implications for crustal evolution. Lithos 79, 1–24. https://doi.org/10.1016/j.lithos.2004.04.048

Martin, H., 1999. Adakitic magmas: Modern analogues of Archaean granitoids. Lithos 46, 411–429. https://doi.org/10.1016/S0024-4937(98)00076-0

Mayne M.J, Stevens G., Moyen J-F., 2020. A phase equilibria investigation of selected source controls on the composition of melt batches generated by sequential melting of an average metapelite.. From: Janousek, V., Bonin, B., Collins, W.J., Farina, F., Bowden, P (eds) 2020. Post-Archean Granitic rocks: Petrogenetic Processes and Tectonic Environments. Geological society of London, Special Pubblication, 491, 223-241.

McDonough, W.F., Sun, S. s., 1995. The composition of the Earth. Chem. Geol. 120, 223–253. https://doi.org/10.1016/0009-2541(94)00140-4

Journal Pre-proof

Miller, J.S., Matzel, J.E.P., Miller, C.F., Burgess, S.D., Miller, R.B., 2007. Zircon growth and recycling during the assembly of large, composite arc plutons. J. Volcanol. Geotherm. Res. 167, 282–299. https://doi.org/10.1016/j.jvolgeores.2007.04.019

Narduzzi F., Farina F., Stevens G., Lana C., Nalini Jr H.A., 2017. Magmatic garnet in the Cordilleran-type Galiléia granitoids of the Araçuaí belt (Brazil): Evidence for crystallization in the lower crust. Lithos, 282-283, 82-97.

Plank, T., Langmuir, C.H., 1998. The chemical composition of subducting sediment and its consequences for the crust and mantle. Chem. Geol. 145, 325–394. https://doi.org/10.1016/S0009-2541(97)00150-2

Plank, T., 2005. Constraints from Thorium/Lanthanum on sediment recycling at subduction zones and the evolution of the continents. J. Petrol. 46, 921–944. https://doi.org/10.1093/petrology/egi005

Plank, T., 2014. The Chemical Composition of Subducting Sediments. In: Holland, H.D., Turekian, K.K. (Eds.), Treatise on Geochemistry, The Crust, 2nd ed. Elsevier, Amsterdam, pp. 607-629. https://doi.org/10.1016/B978-0-08-095975-7.00319-3.

Quick, J.E., Sinigoi, S., Snoke, A.W., Kalakay, T.J., Mayer, A., Peressini, G., 2002. Geologic map of the southern Ivrea-Verbano Zone, northwestern Italy.

Relvini, A., Martin, S., Carvalho, B.B., Prosser, G., Toffolo, L., Macera, P., Bartoli, O., 2022. Genesis of the Eastern Adamello Plutons (Northern Italy): Inferences for the Alpine Geodynamics. Geosci. 12. https://doi.org/10.3390/geosciences12010013

Rustioni, G., Audetat, A., Keppler, H., 2021. The composition of subduction zone fluids and the origin of the trace element enrichment in arc magmas. Contrib. to Mineral. Petrol. 176, 1–19. https://doi.org/10.1007/s00410-021-01810-8

Schaltegger, U., Brack, P., Ovtcharova, M., Peytcheva, I., Schoene, B., Stracke, A., ... & Bargossi, G. M. (2009). Zircon and titanite recording 1.5 million years of magma accretion, crystallization and initial cooling in a composite pluton (southern Adamello batholith, northern Italy). Earth and Planetary Science Letters, 286(1-2), 208-218.

Schaltegger, U., Nowak, A., Ulianov, A., Fisher, C.M., Gerdes, A., Spikings, R., Whitehouse, M.J., Bindeman, I., Hanchar, J.M., Duff, J., Vervoort, J.D., Sheldrake, T., Caricchi, L., Brack, P., Müntener, O., 2019. Zircon Petrochronology and 40Ar/39Ar Thermochronology of the Adamello Intrusive Suite, N. Italy:

Journal Pre-proof

Monitoring the Growth and Decay of an Incrementally Assembled Magmatic System. J. Petrol. 60, 701–722. https://doi.org/10.1093/petrology/egz010

Schettino, E., Poli, S., 2020. Hydrous Carbonatitic Liquids Drive CO2 Recycling From Subducted Marls and Limestones. Geophys. Monogr. Ser. 249, 209–221. https://doi.org/10.1002/9781119508229.ch18

Schmidt, M.W., Poli, S., 2004. Magmatic epidote. Rev. Mineral. Geochemistry 56, 399–430. https://doi.org/10.2138/gsrmg.56.1.399

Schoene, B., Schaltegger, U., Brack, P., Latkoczy, C., Stracke, A., Günther, D., 2012. Rates of magma differentiation and emplacement in a ballooning pluton recorded by U–Pb TIMS-TEA, Adamello batholith, Italy. Earth Planet. Sci. Lett. 355–356, 162–173. https://doi.org/10.1016/j.epsl.2012.08.019

Shirey, S.B., Hanson, G.N., 1984. Mantle-derived Archaean monozodiorites and trachyandesites. Nature 310, 222–224. https://doi.org/10.1038/310222a0

Sial, A.N., Vasconcelos, P.M., Ferreira, V.P., Pessoa, R.R., Brasilino, R.G., Morais Neto, J.M., 2008. Geochronological and mineralogical constraints on depth of emplacement and ascencion rates of epidote-bearing magmas from northeastern Brazil. Lithos 105, 225–238. https://doi.org/10.1016/j.lithos.2008.04.002

Sinigoi, S., Quick, J.E., Clemens-Knott, D., Mayer, A., Demarchi, G., Mazzucchelli, M., Negrini, L., Rivalenti, G., 1994. Chemical evolution of a large mafic intrusion in the lower crust, Ivrea-Verbano Zone, northern Italy. J. Geophys. Res. Solid Earth 99, 21575–21590.

Sun, W., Zhao, L., Malusà, M.G., Guillot, S., Fu, L.Y., 2019. 3-D Pn tomography reveals continental subduction at the boundaries of the Adriatic microplate in the absence of a precursor oceanic slab. Earth Planet. Sci. Lett. 510, 131–141. https://doi.org/10.1016/j.epsl.2019.01.012

Syracuse, E.M., van Keken, P.E., Abers, G.A., Suetsugu, D., Bina, C., Inoue, T., Wiens, D., Jellinek, M., 2010. The global range of subduction zone thermal models. Phys. Earth Planet. Inter. 183, 73–90. https://doi.org/10.1016/j.pepi.2010.02.004

Tiepolo, M., Tribuzio, R., 2005. Slab-melting during Alpine orogeny: Evidence from mafic cumulates of the Adamello batholith (Central Alps, Italy). Chem. Geol. 216, 271–288. https://doi.org/10.1016/j.chemgeo.2004.11.014

Journal Pre-proof

Tiepolo, M., Tribuzio, R., Ji, W.Q., Wu, F.Y., Lustrino, M., 2014. Alpine Tethys closure as revealed by amphibole-rich mafic and ultramafic rocks from the Adamello and the Bergell intrusions (Central Alps). J. Geol. Soc. London. 171, 793–799. https://doi.org/10.1144/jgs2013-139

Tiepolo, M., Tribuzio, R., Langone, A., 2011. High-mg andesite petrogenesis by amphibole crystallization and ultramafic crust assimilation: Evidence from Adamello hornblendites (Central Alps, Italy). J. Petrol. 52, 1011–1045. https://doi.org/10.1093/petrology/egr016

Ulmer, P., Callegari, E., Sonderegger, U.C., 1983. Genesis of the mafic and ultramafic rocks and their genetical relations to the tonalitic-trondhjemitic granitoids of the southern part of the Adamello Batholith (Northern Italy). Mem. Soc. Geol. It. 26, 171–222.

Veizer, J., Mackenzie, F.T., 2003. Evolution of sedimentary rocks. Treatise on Geochemistry, vol. 7. Elsevier-Pergamon, Oxford, pp. 369-407.

Vervoort, J.D., Plank, T., Prytulak, J., 2011. The Hf-Nd isotopic composition of marine sediments. Geochim. Cosmochim. Acta 75, 5903–5926. https://doi.org/10.1016/j.gca.2011.07.046

Vervoort, J.D., Kemp, A.I.S., 2016. Clarifying the zircon Hf isotope record of crust-mantle evolution. Chem. Geol. 425, 65–75. https://doi.org/10.1016/j.chemgeo.2016.01.023

Visonà, D., Caironi, V., Carraro, A., Dallai, L., Fioretti, A.M., Fanning, M., 2007. Zircon megacrysts from basalts of the Venetian Volcanic Province (NE Italy): U–Pb ages, oxygen isotopes and REE data. Lithos 94, 168–180. https://doi.org/10.1016/j.lithos.2006.06.007

Wang, L., Hu, W., Wang, X., Cao, J., Yao, S., 2020. Halogens (Cl, Br, and I) geochemistry in Middle Triassic carbonates: Implications for salinity and diagenetic alteration of I/(Ca+ Mg) ratios. Chem. Geol. 533, 119444.

Zaccaria, D., Vicentini, N., Perna, M.G., Rosatelli, G., Sharygin, V. V., Humphreys-Williams, E., Brownscombe, W., Stoppa, F., 2021. Lamprophyre as the source of zircon in the Veneto region, Italy. Minerals 11, 1–28. https://doi.org/10.3390/min11101081

Journal Pre-proof

Journal Pre-proof

Declaration of interests

☒The authors declare that they have no known competing financial interests or personal relationships that could have appeared to influence the work reported in this paper.

☐The authors declare the following financial interests/personal relationships which may be considered as potential competing interests:

Journal Pre-proof

Journal Pre-proof

Highlights

- The Corno Alto complex consists of three types of granitoid rocks
- The Corno Alto complex is chemically peculiar in the Adamello framework
- High Ba content likely derived from melting of carbonate sediments of slab origin
- The Corno Alto complex is a modern analogue of the high Ba/K sanukitoids

Journal Pre-proof

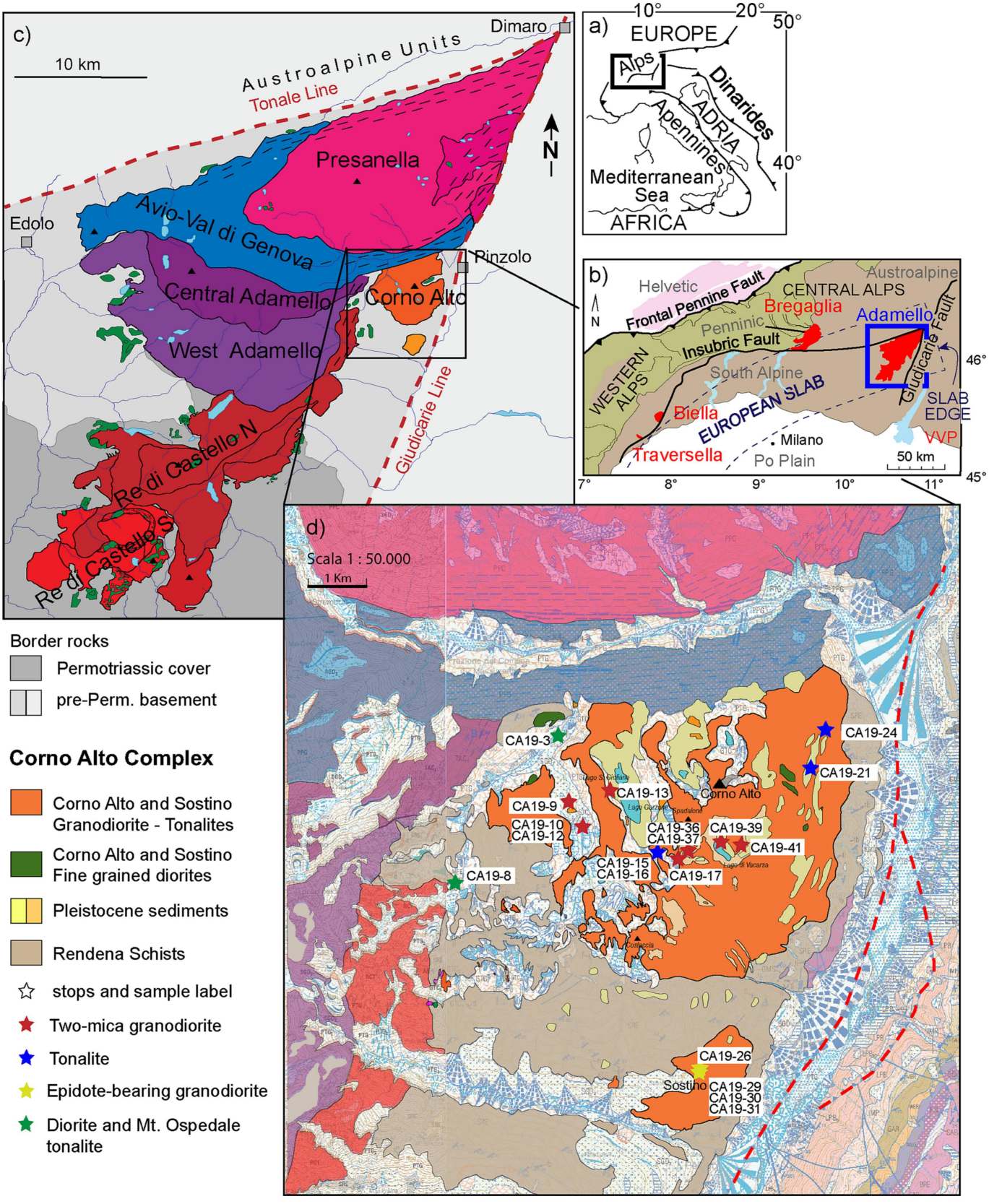
c)
10 km
Austroalpine Units
Tonale Line
Dimaro
Presanella
N
Edolo
Avio-Val di Genova
Pinzolo
Central Adamello
Corno Alto
West Adamello
Giudicarie Line
Re di Castello N
Re di Castello S
a)
10°
20°
50°
EUROPE
Alps
Dinarides
ADRIA
Apennines
40°
Mediterranean Sea
AFRICA
b)
N
Helvetic
Frontal Pennine Fault
CENTRAL ALPS
Austroalpine
Bregaglia
Adamello
Penninic
Insubric Fault
Giudicarie Fault
WESTERN ALPS
South Alpine
46°
EUROPEAN SLAB
SLAB EDGE
Biella
VVP
Milano
Traversella
Po Plain
50 km
45°
7°
8°
9°
10°
11°
d)
Scala 1 : 50.000
1 Km
CA19-3
CA19-24
CA19-21
CA19-13
Corno Alto
CA19-9
CA19-10
CA19-12
CA19-36
CA19-37
CA19-39
CA19-41
CA19-15
CA19-16
CA19-17
CA19-8
CA19-26
Sostino
CA19-29
CA19-30
CA19-31
Border rocks
Permotriassic cover
pre-Perm. basement
Corno Alto Complex
Corno Alto and Sostino Granodiorite - Tonalites
Corno Alto and Sostino Fine grained diorites
Pleistocene sediments
Rendena Schists
stops and sample label
Two-mica granodiorite
Tonalite
Epidote-bearing granodiorite
Diorite and Mt. Ospedale tonalite

Figure 1

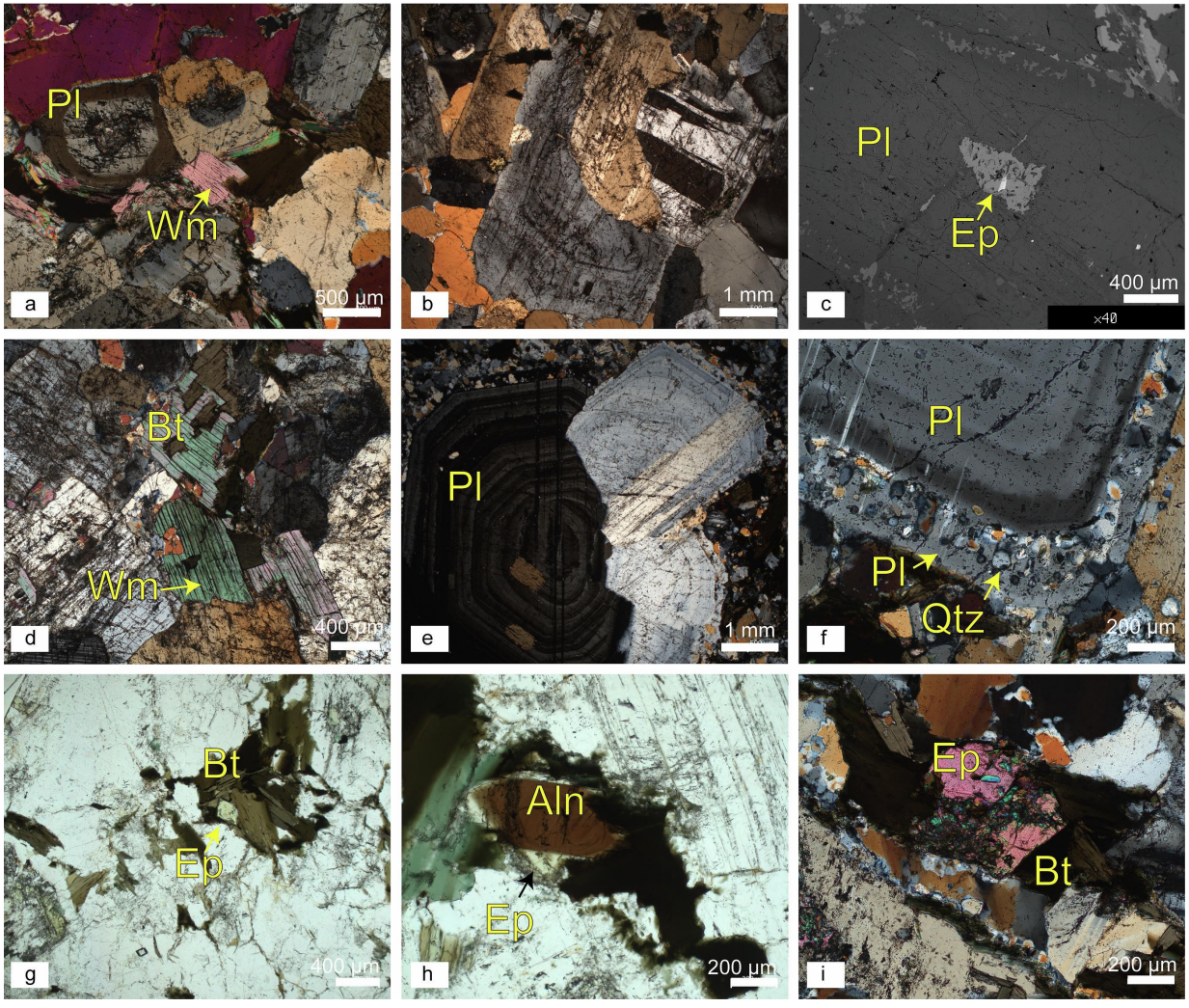
Pl
Wm
a
500 µm
b
1 mm
Pl
Ep
400 µm
×40
c
Bt
Wm
d
400 µm
Pl
e
1 mm
Pl
Pl
Qtz
f
200 µm
Bt
Ep
g
400 µm
Aln
Ep
h
200 µm
Ep
Bt
i
200 µm

Figure 2

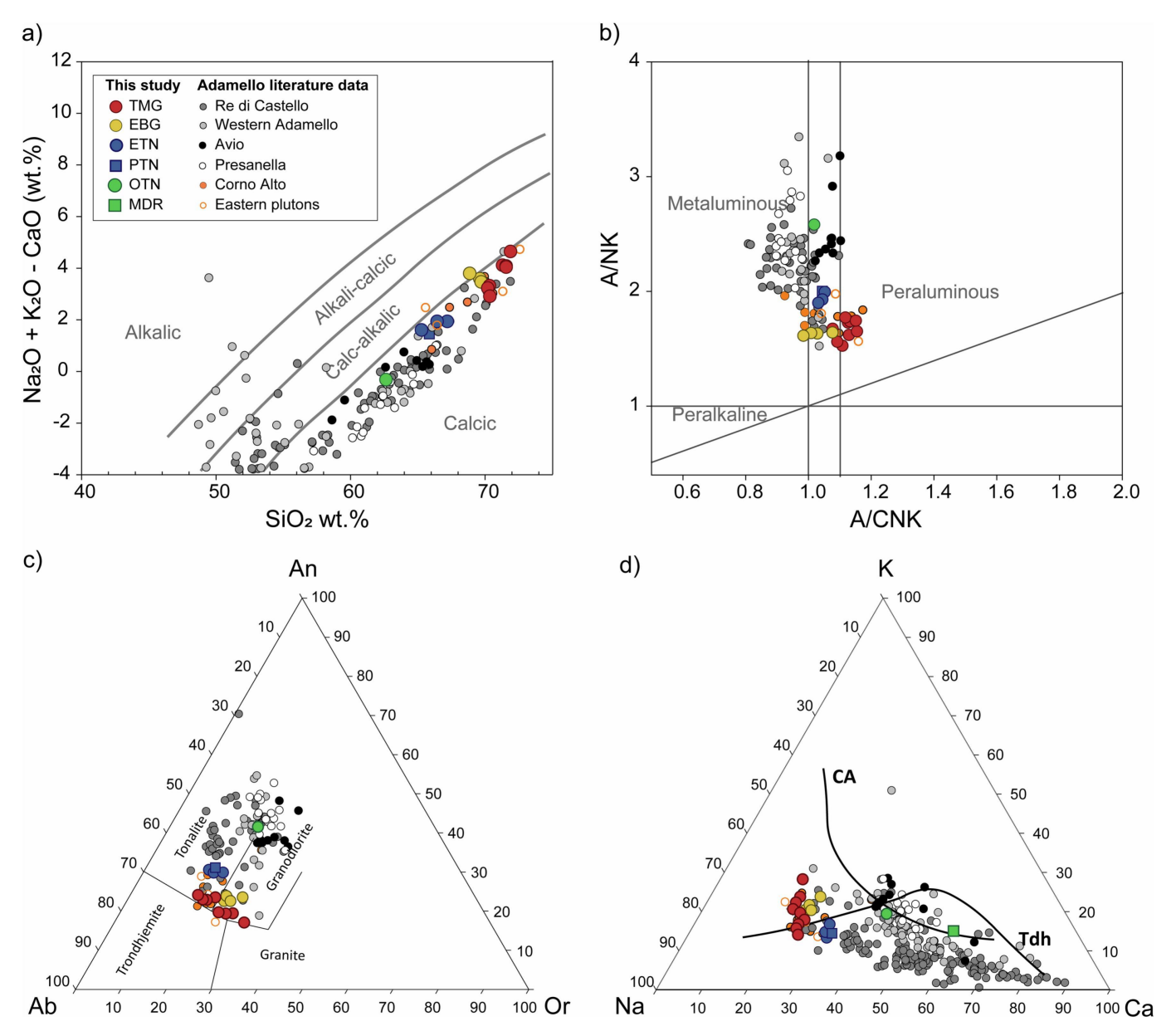
a)
This study
TMG
EBG
ETN
PTN
OTN
MDR
Adamello literature data
Re di Castello
Western Adamello
Avio
Presanella
Corno Alto
Eastern plutons
Alkalic
Alkali-calcic
Calc-alkalic
Calcic
Na2O + K2O - CaO (wt.%)
SiO2 wt.%
b)
Metaluminous
Peraluminous
Peralkaline
A/NK
A/CNK
c)
An
Ab
Or
Tonalite
Granodiorite
Trondhjemite
Granite
d)
K
Na
Ca
CA
Tdh

Figure 3

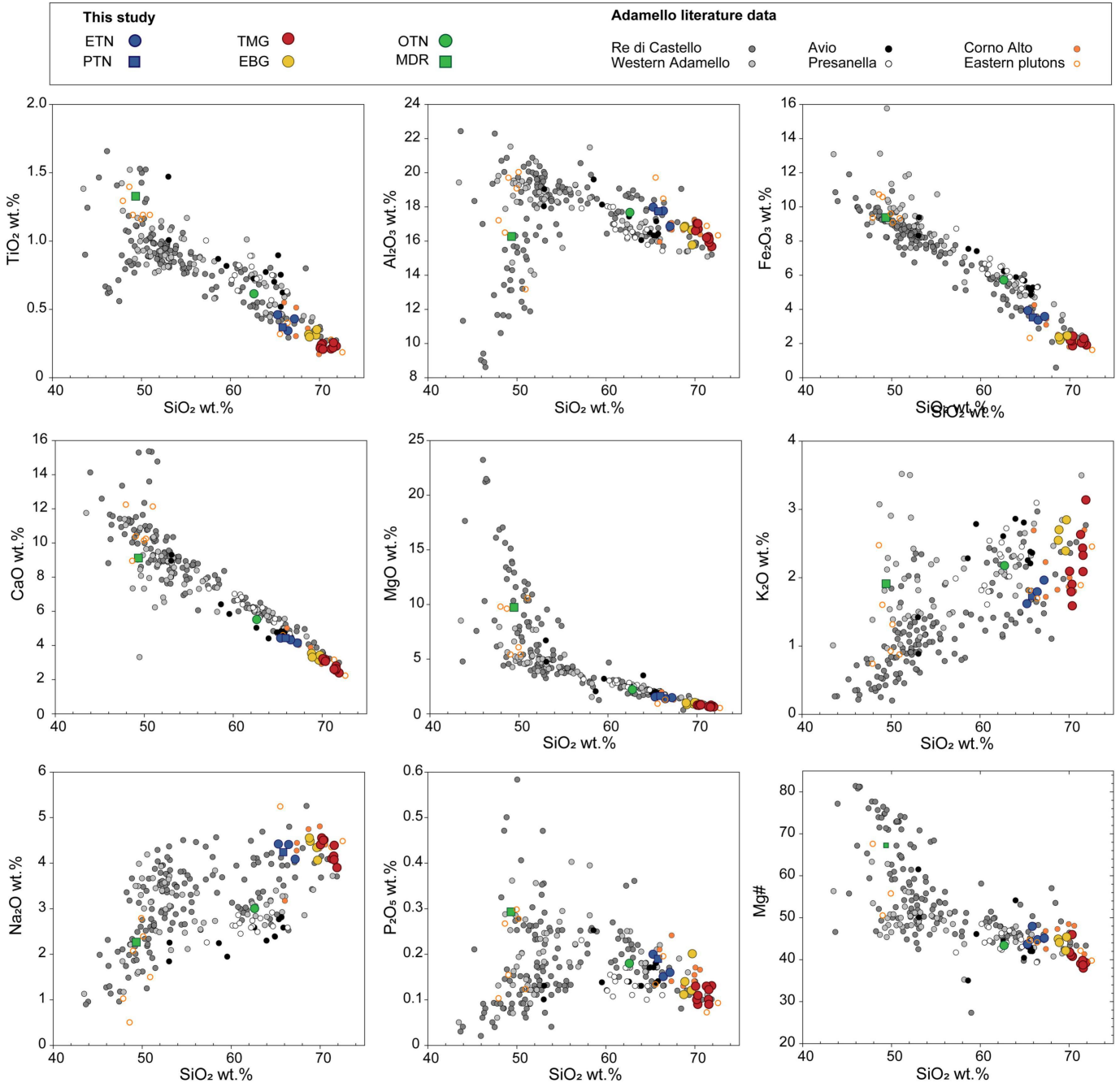
This study
ETN
PTN
TMG
EBG
OTN
MDR
Adamello literature data
Re di Castello
Western Adamello
Avio
Presanella
Corno Alto
Eastern plutons
TiO2 wt.%
Al2O3 wt.%
Fe2O3 wt.%
CaO wt.%
MgO wt.%
K2O wt.%
Na2O wt.%
P2O5 wt.%
Mg#
SiO2 wt.%

Figure 4

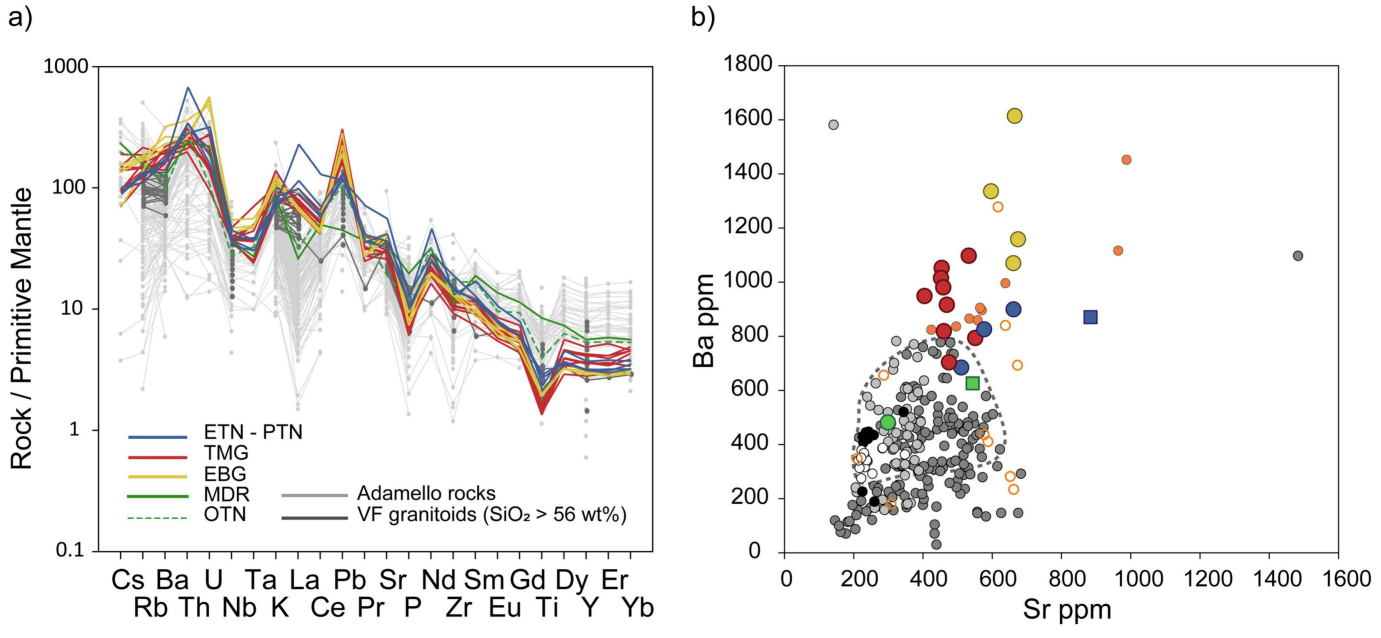
a)
b)
Rock / Primitive Mantle
1000
100
10
1
0.1
Cs Ba U Ta La Pb Sr Nd Sm Gd Dy Er
Rb Th Nb K Ce Pr P Zr Eu Ti Y Yb
ETN - PTN
TMG
EBG
MDR
OTN
Adamello rocks
VF granitoids (SiO2 > 56 wt%)
Ba ppm
1800
1600
1400
1200
1000
800
600
400
200
0
0 200 400 600 800 1000 1200 1400 1600
Sr ppm

Figure 5

A-Type domains

Oscillatory zoned cores and rims.
The core-rim boundary is linear or only slightly resorbed.
Medium- to low- luminescence.

**42.6 ± 2 Ma
**$\varepsilon Hf_{(i)}$: +5.0 ± 1.1

*45.3 ± 1.4 Ma
**44.5 ± 1.24 Ma
*$\varepsilon Hf_{(i)}$: +6.7 ± 1.3
**$\varepsilon Hf_{(i)}$: +6.4 ± 1.7

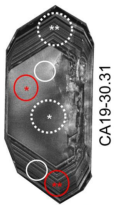

* 44.1 ± 1.8 Ma
** 44.7 ± 2.2 Ma
* $\varepsilon Hf_{(i)}$: +5.3 ± 0.9
**$\varepsilon Hf_{(i)}$: +4.8 ± 0.8

B-Type domains

Unzoned to weakly zoned domains, displaying a dissolution surface at their boundary. Medium luminescence.

*43.6 ± 1.5 Ma
**43.2 ± 1.2 Ma
*$\varepsilon Hf_{(i)}$: +14.1 ± 1.9

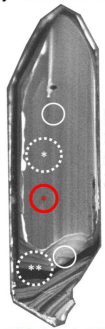

*42.3 ± 1.4 Ma
*$\varepsilon Hf_{(i)}$ +13.3 ± 1.7
**$\varepsilon Hf_{(i)}$ +7.5 ± 1.0

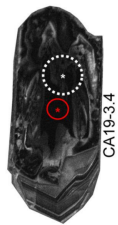

*44.8 ± 1.4 Ma
*$\varepsilon Hf_{(i)}$ 11.9 ± 1.4

C-Type domains

Rounded and bright-CL cores with possible overgrowth of discordant oscillatory zoned rims (A-type domains).

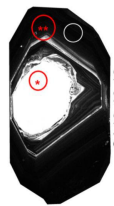

*661 ± 13 Ma
**44.1 ± 0.9 Ma

**463 ± 22 Ma
*42.6 ± 2.2 Ma

50 µm

U-Pb

Trace elements

Lu-Hf

Figure 6

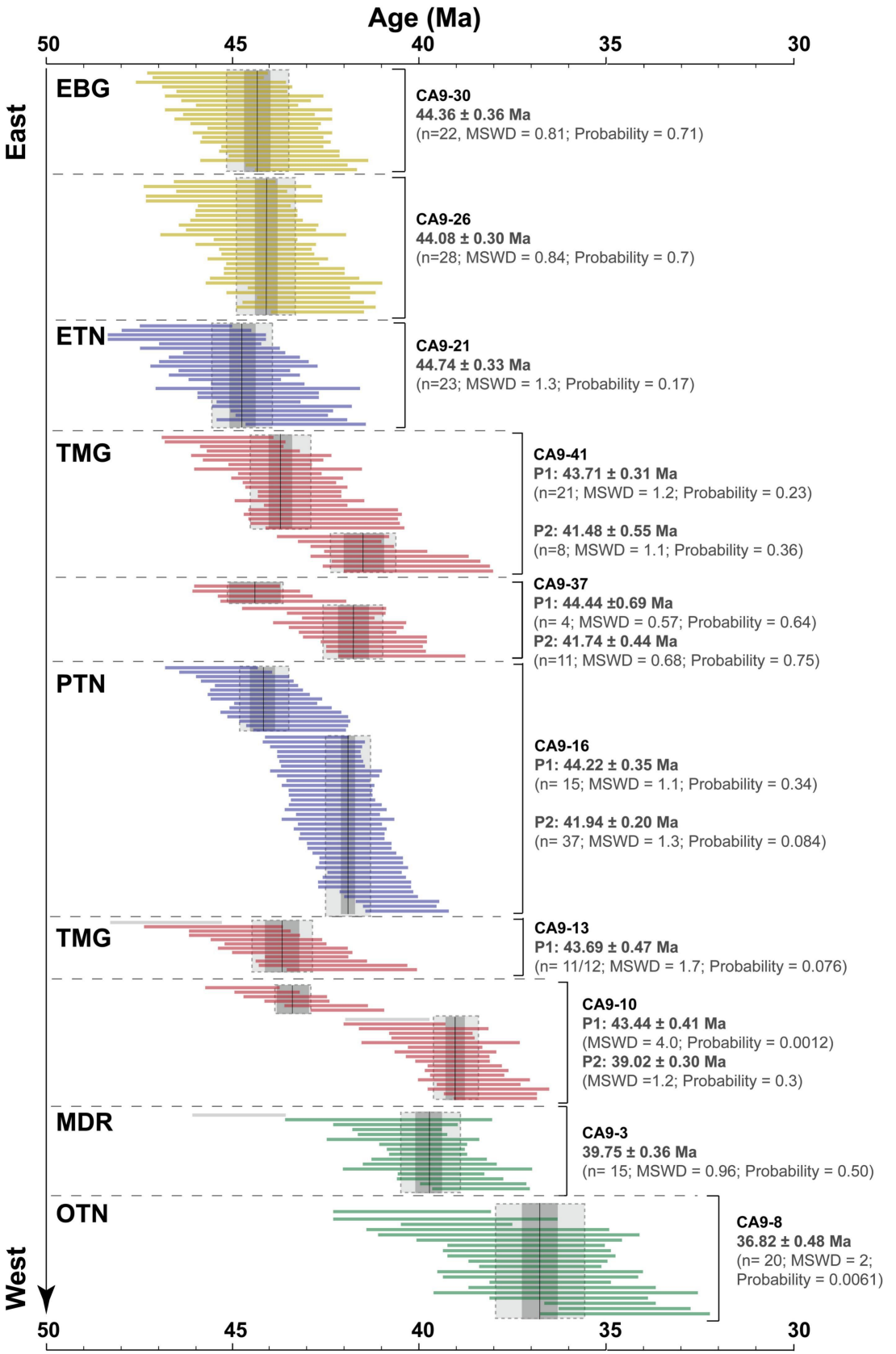
Age (Ma)
50
45
40
35
30
East
West
EBG
CA9-30
44.36 ± 0.36 Ma
(n=22, MSWD = 0.81; Probability = 0.71)
CA9-26
44.08 ± 0.30 Ma
(n=28; MSWD = 0.84; Probability = 0.7)
ETN
CA9-21
44.74 ± 0.33 Ma
(n=23; MSWD = 1.3; Probability = 0.17)
TMG
CA9-41
P1: 43.71 ± 0.31 Ma
(n=21; MSWD = 1.2; Probability = 0.23)
P2: 41.48 ± 0.55 Ma
(n=8; MSWD = 1.1; Probability = 0.36)
CA9-37
P1: 44.44 ±0.69 Ma
(n= 4; MSWD = 0.57; Probability = 0.64)
P2: 41.74 ± 0.44 Ma
(n=11; MSWD = 0.68; Probability = 0.75)
PTN
CA9-16
P1: 44.22 ± 0.35 Ma
(n= 15; MSWD = 1.1; Probability = 0.34)
P2: 41.94 ± 0.20 Ma
(n= 37; MSWD = 1.3; Probability = 0.084)
TMG
CA9-13
P1: 43.69 ± 0.47 Ma
(n= 11/12; MSWD = 1.7; Probability = 0.076)
CA9-10
P1: 43.44 ± 0.41 Ma
(MSWD = 4.0; Probability = 0.0012)
P2: 39.02 ± 0.30 Ma
(MSWD =1.2; Probability = 0.3)
MDR
CA9-3
39.75 ± 0.36 Ma
(n= 15; MSWD = 0.96; Probability = 0.50)
OTN
CA9-8
36.82 ± 0.48 Ma
(n= 20; MSWD = 2;
Probability = 0.0061)

Figure 7

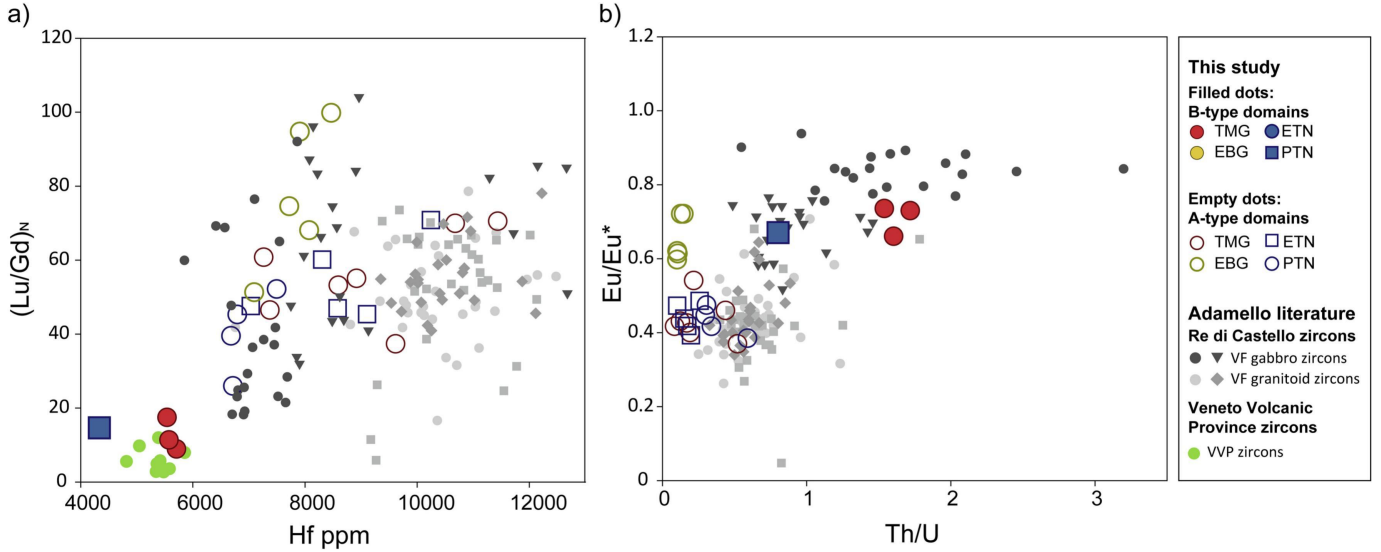
a)
b)
(Lu/Gd)N
Hf ppm
Eu/Eu*
Th/U
This study
Filled dots:
B-type domains
TMG
ETN
EBG
PTN
Empty dots:
A-type domains
TMG
ETN
EBG
PTN
Adamello literature
Re di Castello zircons
VF gabbro zircons
VF granitoid zircons
Veneto Volcanic Province zircons
VVP zircons

Figure 8

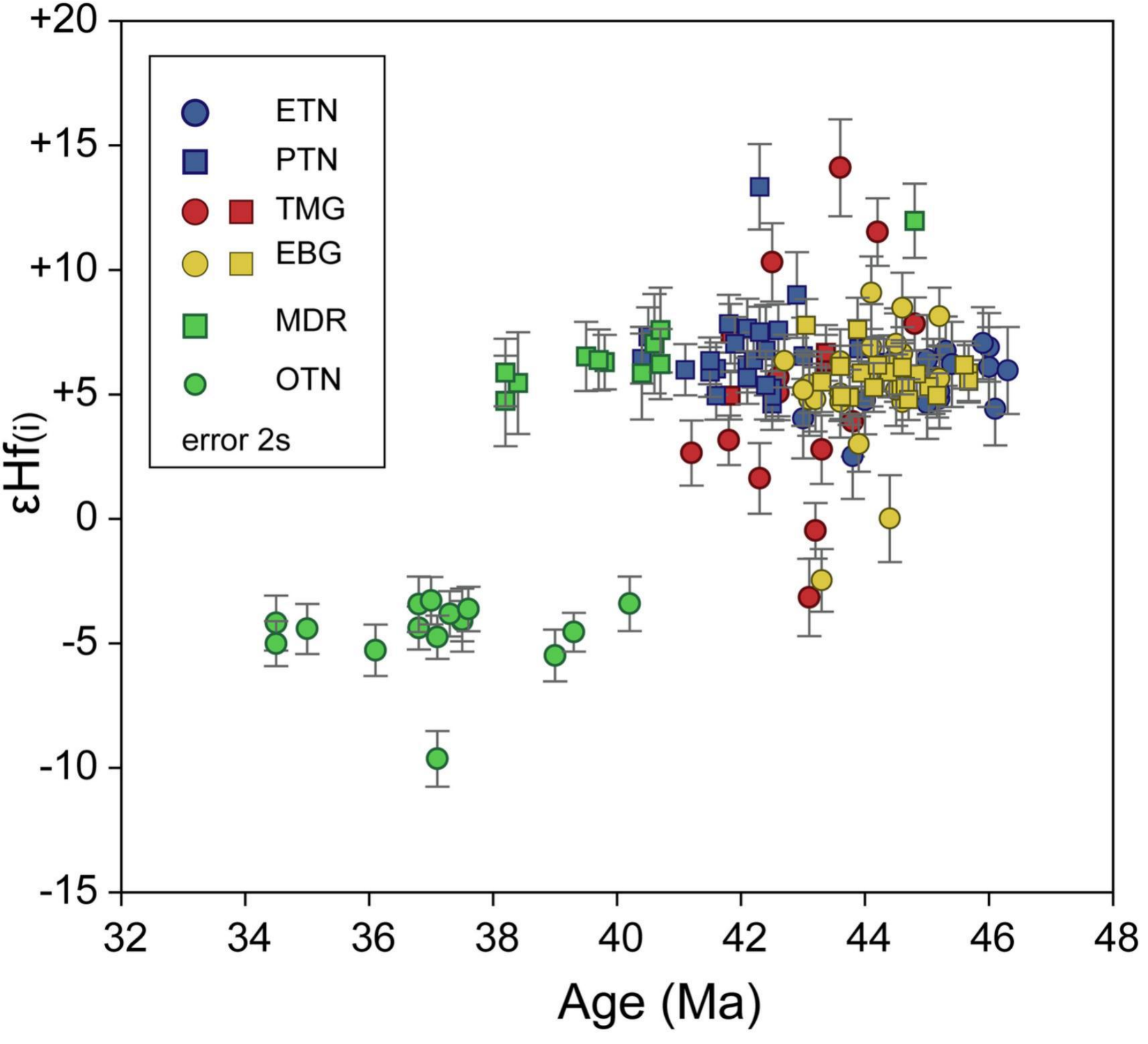
+20
+15
+10
+5
0
-5
-10
-15
εHf(i)
32
34
36
38
40
42
44
46
48
Age (Ma)
ETN
PTN
TMG
EBG
MDR
OTN
error 2s

Figure 9

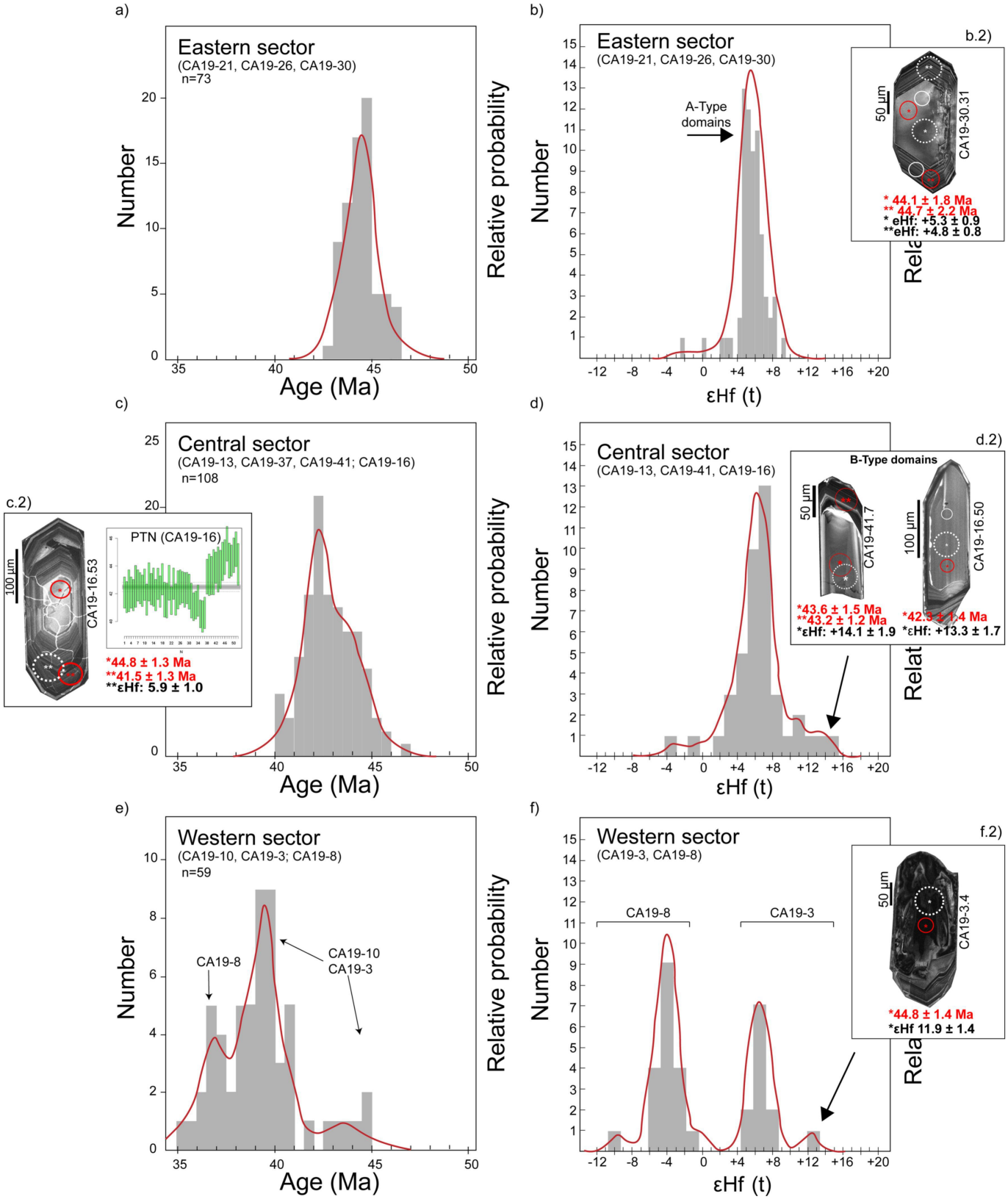
a)
Eastern sector
(CA19-21, CA19-26, CA19-30)
n=73
Number
Age (Ma)
Relative probability
b)
Eastern sector
(CA19-21, CA19-26, CA19-30)
A-Type domains
Number
εHf (t)
b.2)
50 µm
CA19-30.31
* 44.1 ± 1.8 Ma
** 44.7 ± 2.2 Ma
* eHf: +5.3 ± 0.9
**eHf: +4.8 ± 0.8
c)
Central sector
(CA19-13, CA19-37, CA19-41; CA19-16)
n=108
Number
Age (Ma)
Relative probability
c.2)
100 µm
CA19-16.53
PTN (CA19-16)
*44.8 ± 1.3 Ma
**41.5 ± 1.3 Ma
**εHf: 5.9 ± 1.0
d)
Central sector
(CA19-13, CA19-41, CA19-16)
Number
εHf (t)
d.2)
B-Type domains
50 µm
CA19-41.7
*43.6 ± 1.5 Ma
**43.2 ± 1.2 Ma
*εHf: +14.1 ± 1.9
100 µm
CA19-16.50
*42.3 ± 1.4 Ma
*εHf: +13.3 ± 1.7
e)
Western sector
(CA19-10, CA19-3; CA19-8)
n=59
CA19-8
CA19-10
CA19-3
Number
Age (Ma)
Relative probability
f)
Western sector
(CA19-3, CA19-8)
CA19-8
CA19-3
Number
εHf (t)
f.2)
50 µm
CA19-3.4
*44.8 ± 1.4 Ma
*εHf 11.9 ± 1.4

Figure 10

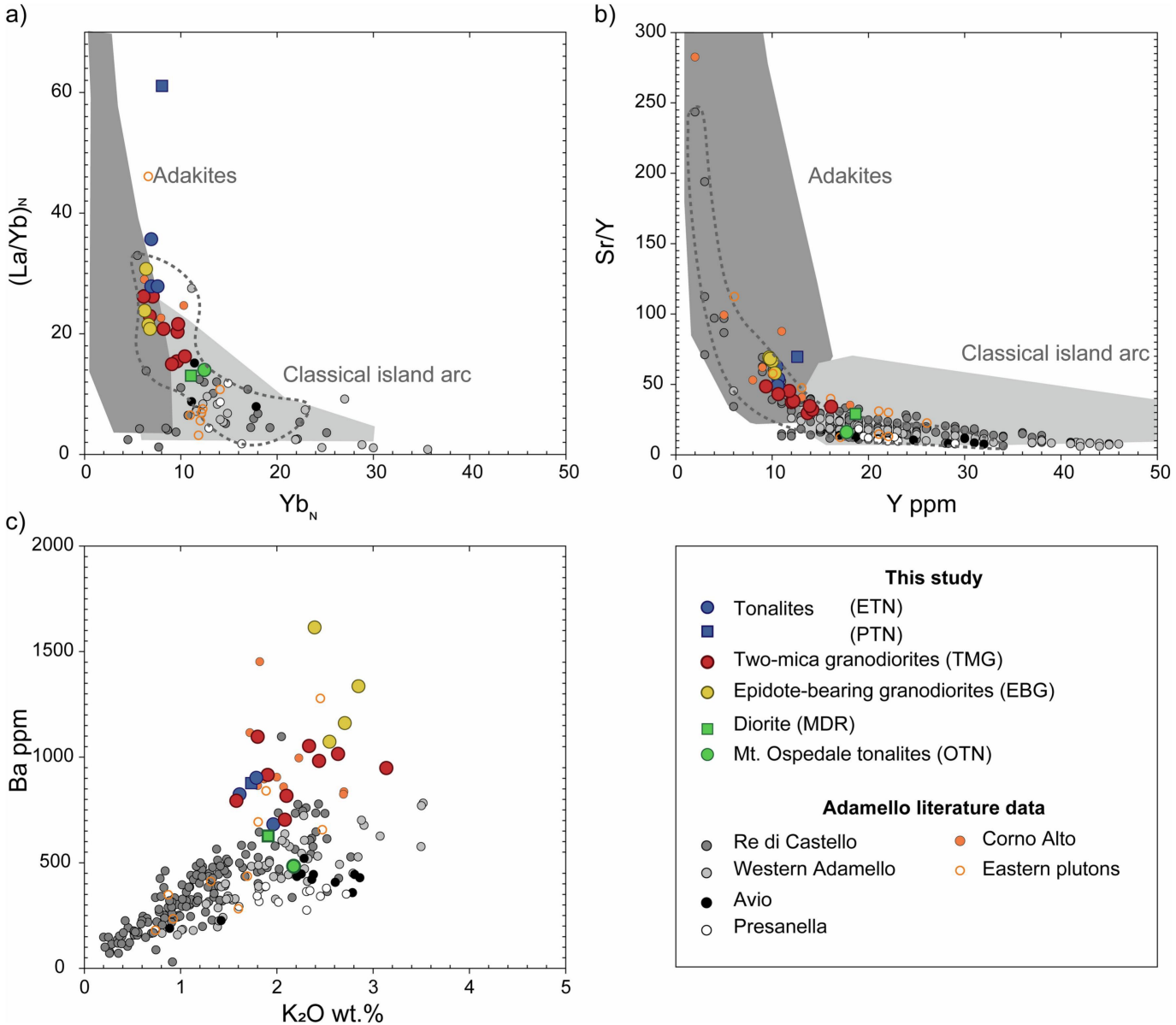
a)
(La/Yb)N
Yb N
Adakites
Classical island arc
b)
Sr/Y
Y ppm
Adakites
Classical island arc
c)
Ba ppm
K2O wt.%
This study
Tonalites (ETN)
(PTN)
Two-mica granodiorites (TMG)
Epidote-bearing granodiorites (EBG)
Diorite (MDR)
Mt. Ospedale tonalites (OTN)
Adamello literature data
Re di Castello
Western Adamello
Avio
Presanella
Corno Alto
Eastern plutons

Figure 11

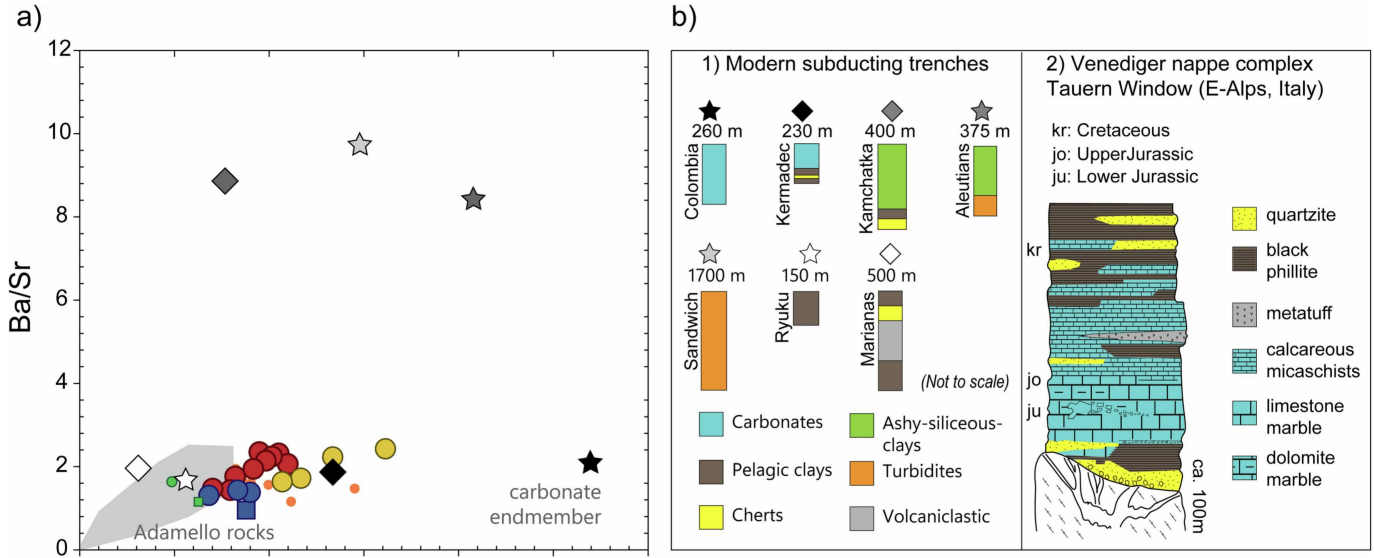
a)
Ba/Sr
Ba ppm
Adamello rocks
carbonate
endmember
b)
1) Modern subducting trenches
260 m
Colombia
230 m
Kermadec
400 m
Kamchatka
375 m
Aleutians
1700 m
Sandwich
150 m
Ryuku
500 m
Marianas
(Not to scale)
Carbonates
Ashy-siliceous-clays
Pelagic clays
Turbidites
Cherts
Volcaniclastic
2) Venediger nappe complex
Tauern Window (E-Alps, Italy)
kr: Cretaceous
jo: UpperJurassic
ju: Lower Jurassic
kr
jo
ju
ca. 100m
quartzite
black phillite
metatuff
calcareous micaschists
limestone marble
dolomite marble

Figure 12

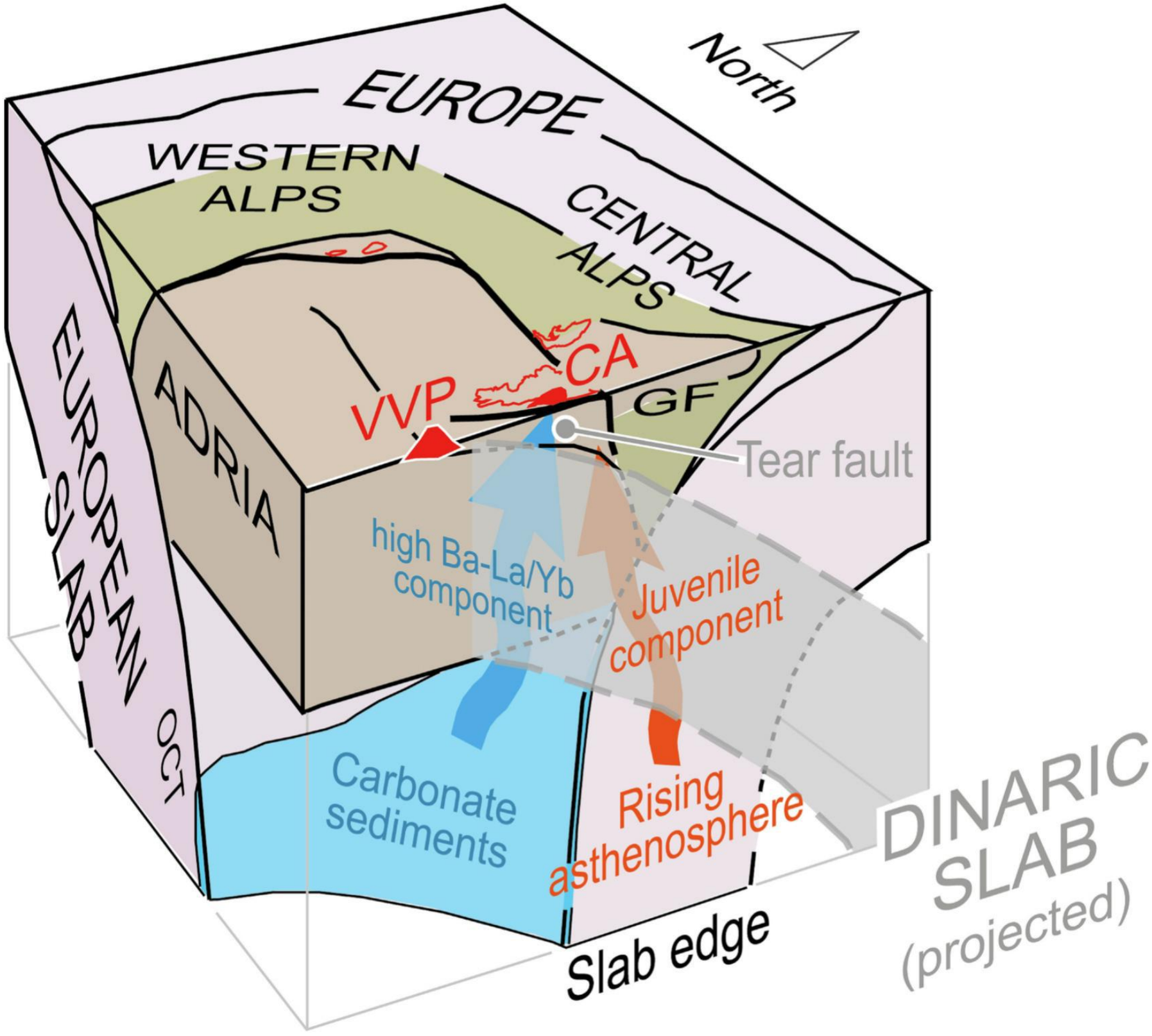
North
EUROPE
WESTERN ALPS
CENTRAL ALPS
ADRIA
EUROPEAN SLAB
OCT
CA
VVP
GF
Tear fault
high Ba-La/Yb component
Juvenile component
Carbonate sediments
Rising asthenosphere
Slab edge
DINARIC SLAB (projected)

Figure 13